Univerzita Karlova

Přírodovědecká fakulta

Studijní program: Fyziologie živočichů

Studijní obor: Fyziologie živočichů a člověka

Bc. Kristýna Kováčová

Kódování feromonového signálu olfaktorními neurony motýla *Agrotis ipsilon*

Coding of pheromone signal by olfactory receptor neurons in *Agrotis ipsilon*

Diplomová práce

Vedoucí diplomové práce: Mgr. Lubomír Košťál, Ph.D.

Praha 2022

Prohlašuji, že jsem závěrečnou práci zpracovala samostatně a že jsem uvedla všechny použité informační zdroje a literaturu. Tato práce ani její podstatná část nebyla předložena k získání jiného nebo stejného akademického titulu.

V Praze, 8. 7. 2022

Děkuji svému školiteli, Lubomíru Košťálovi, za vstřícný přístup a ochotu, s kterou mne vedl při vypracovávání diplomového projektu, a za mnohé cenné rady, jež mi poskytl. Rovněž jsem velice vděčná své rodině za to, že mne během celého studia podporovala.

Abstrakt a klíčová slova

Hlavním cílem této diplomové práce je popsat, zdali a jak se liší aktivita olfaktorních recepčních neuronů u samců *A. ipsilon* při stimulaci samičím pohlavním feromonem s různou časovou dynamikou koncentrace, tedy buďto umělým konstantním pulsem nebo přerušovaným signálem podobným přirozené stimulaci. Za tímto účelem byla ve spolupracující laboratoři (Dr. P. Lucas, INRAe, Versailles, France) získána experimentální data za použití nového olfaktometrického systému umožňujícího přesnou kontrolu nad časováním dodávek feromonu k sensillu. Byla provedena analýza odpovědi pomocí řady různých kvantifikátorů spolehlivosti, náhodnosti a variability v programovacím jazyce R. Výsledky byly interpretovány v kontextu klasické hypotézy efektivního kódování, která říká, že senzorické neurony jsou evolučně adaptovány na přirozenou stimulaci. Hlavní zjištění je, že ačkoli variabilita odpovědi celé populace ORN na fluktuující nebo konstantní stimulaci se ne vždy liší, na úrovni individuálních neuronů je odpověď na fluktuující stimulaci zpravidla méně variabilní, a tedy spolehlivější, než na stimulaci konstantní. Diplomová práce rovněž shrnuje důležitá fakta a hypotézy týkající se neuronálního kódování a olfakce u *Lepidoptera*.

Klíčová slova: početní neurovědy, neuronální kódování, feromon, *Agrotis ipsilon*, olfaktorní recepční neuron, biofyzikální modelování

Abstract and keywords

The main objective of the thesis is to describe differences in the activity of male *A. ipsilon* olfactory receptor neurons (ORNs) when stimulated by different temporal dynamics of the concentration of the conspecific female pheromone. First, under the artificial situation of constant pulse stimulation, and second, with a fluctuating signal resembling the natural situation. For this purpose, the experimental data were collected in the collaborating laboratory (Dr. P. Lucas, INRAe, Versailles, France) by employing a novel olfactometer system that enables precise temporal control of the pheromone delivery to individual sensilla. Using the R programming language, we analyzed various descriptors of the response reliability, randomness, and variability, as well as the information content of the evoked activity. The results are interpreted in the context of the classical efficient coding hypothesis, which states that sensory neurons are evolutionarily adapted to natural stimuli. The main finding is that although the response variability is widely spread across the ORN population, sometimes with no visible difference between the constant and fluctuating stimulation types, the fluctuating stimulus is usually encoded with systematically higher reliability, as revealed by the inspection of individual ORNs. The thesis also summarizes the main facts and hypotheses concerning neuronal coding and olfaction in *Lepidoptera.*

Keywords: computational neuroscience, neural coding, pheromone, *Agrotis ipsilon*, olfactory receptor neuron, biophysical modeling

Table of contents

List of abbreviations

CV	coefficient of variation
DAG	diacylglycerol
$ECDF$	empirical cumulative distribution function
$GPCR$	G-protein coupled receptors
$IP3$	inositol trisphosphate
IQR	interquartile range
ISI	inter-spike interval
LV	local variation
MAD	median absolute deviation
OR	odorant receptor
ORN	olfactory receptor neuron
$r.v.$	random variable
PBP	pheromone-binding protein
PDF	probability density function
PLC	phospholipase C
PKC	protein kinase C
PR	pheromone receptor
PRN	pheromone receptor neurons
$PSTH$	peristimulus time histogram
SD	standard deviation
$SNMP1$	sensory neuron membrane protein

1. Introduction

The presented work belongs to a relatively young field of *computational neuroscience*, which essentially seeks to quantitatively explain how neurons represent and process information. We are interested in studying the connection between the characteristics of olfactory stimulation and the variability of the subsequent neural response. More specifically, we study the olfactory receptor neurons in the moth *Agrotis ipsilon* and how they respond to pheromone stimulation with respect to its temporal structure.

2. Literature review

2.1. Computational neuroscience

Computational neuroscience is an interdisciplinary approach to understanding the functional role of neural signals by employing quantitative methods. Biophysical and statistical modeling of the nervous system at different scales, including the cellular and the systems levels, is used complementarily to the traditional neuroscientific techniques. We quote the description of the main goals of computational neuroscience from the eponymously titled paper by Sejnowski, Koch, and Churchland (1988), which helped to establish the subject as a separate field:

"The aim of computational neuroscience is to explain how electrical and chemical signals are used in the brain to represent and process information."

Broadly put, several themes of the current computational neuroscience research were outlined already in the classic Norbert Wiener's 1948 book "Cybernetics: or Control and communication in the animal and the machine", further elaborated in the seminal works of Wiener's collaborators MacKay and McCulloch (1952) and McCulloch and Pitts (1943) and pursued in the classical "Mechanization of Thought Processes: Proceedings of a Symposium Held at the National Physical Laboratory on 24–27$^{\text{th}}$ November 1958".

Nowadays, much more is known about the brain because of advances in experimental neuroscience (both on the micro- and macroscopic levels) and substantial computing power is available for performing realistic simulations of neural systems. Despite the indisputable progress in the much-needed quantitative description of the function of neural systems, we still do not understand precisely how the nervous system plans or makes decisions, remembers, or processes sensory information.

2.2. Neural coding

Neurons are specialized cells that are interconnected by synapses and that can respond to chemical, physical, or mechanical stimuli by sending chemical signals to their synaptic partners. These chemical signals have their origin in the presynaptic axon terminal where they are triggered by action potentials - rapid events of membrane depolarization originating in and traveling from the axon hillock. When the membrane potential of the axon hillock reaches a certain threshold (an occasion whose probability increases greatly with stimulus reception) a fixed and precisely timed series of actions is triggered which leads to further membrane depolarization, as well as the subsequent return to the normal resting potential.

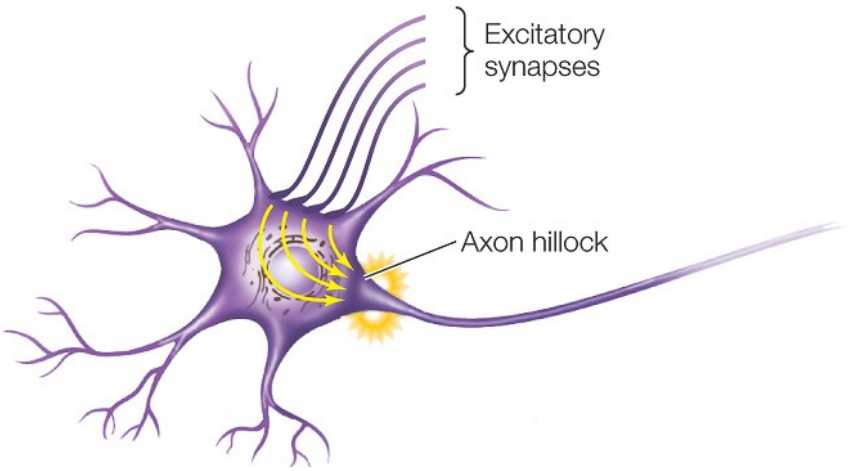

Figure 1: Summation of excitatory presynaptic potentials (EPSPs) at the axon hillock generates action potentials. Taken and adapted from *https://www.macmillanhighered.com/BrainHoney/Resource/6716/digital_first_content/trunk/test/hillis2e/hillis2e_ch34_4.html*.

Thanks to this precise setting, the time course of this event (denoted as the *action potential*) is virtually identical on all occasions (Fig. 1). Moreover, in comparison to an interval between any two subsequent action potentials, the duration of an action potential itself (approximately 1 ms) is usually negligible. For these reasons, we can treat action potentials as identical instantaneous events in which case we call them *spikes*. Membrane potential fluctuations evoked by a stimulus, in other words, the neural response, can be therefore ultimately reduced to a simple list of spike occurrence

time points called the *spike train* (Fig. 1). Since the action potential triggers the synaptic event, all the information about the stimulus that a neuron can transmit further to its synaptic partners is contained within spike trains.

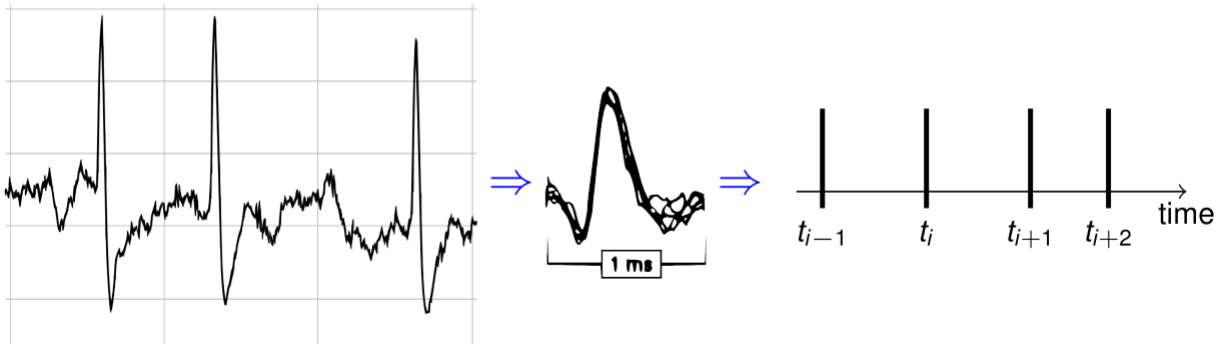

Figure 2: Identity of action potentials simplifies the neural coding assumptions. Extracellular recording of the membrane potential of the olfactory receptor neuron of the moth *Agrotis ipsilon* (left). Individual extracted action potentials are plotted over each other: the shape (time-course of the membrane potential) does not vary significantly (middle). Since the shape of the action potential does not carry additional information besides triggering the synaptic event, the neuronal output can be reduced to a sequence of times when the action potential was fired (right).

The relationship between the stimulus and the subsequent neural response constitutes the fundamental issue that computational neuroscience aims to elucidate (Sejnowski et al., 1988). The study of neural coding involves measuring and characterizing how neurons represent various stimulus characteristics, such as intensity or direction, and their dynamics (Dayan & Abbott, 2005). The set of spike train attributes that neurons use for the representation of these characteristics is called the *neural code*. The subject can be viewed from two opposite standpoints. While the attempt of *neural encoding* is to predict how a neuron will respond to a certain stimulus, *neural decoding* aims to reconstruct a stimulus from a spike sequence it evokes. Either way, the actual neural code is not completely understood and is a subject of active scientific debate. The resolution to the problem highly depends on extensive empirical data, from which the neural code can be more or less precisely estimated or deduced. On top of that, it is also expected to differ among neuronal types (Gerstner & Kistler, 2002). Nevertheless, thanks to extensive research over the last decades, evidence supporting various neural

codes has been gathered. Because none of them is currently accepted unanimously, all neural codes described to date are essentially neural code hypotheses.

Whether a particular code is used by neurons cannot be deduced only from its accuracy (how much information about the stimulus is encoded) or reliability (how much the encoded information differs among trials). Intuitively, one would think that neurons should use the most accurate and reliable code possible, as from the evolutionary point of view it only makes sense (Barlow, 1961). However, we need to be aware that *what is* or *is not* possible is determined by the organism's physiology[1]. Whether a code is physiologically possible can be hard to determine and some neural coding hypotheses, therefore, do not address this issue at all. Nevertheless, all of them can serve as much useful mathematical tools for spike train analysis, including reliability determination.

For example, certain traditional approaches for neural decoding, such as the so-called *maximum-likelihood decoding*, are used frequently and considered to be optimal. However, it is not clear whether such mathematical procedures, which involve advanced numerical operations, are plausible at all for biological systems – and the debate still continues (Deneve, Latham & Pouget, 1999). On the other hand, contemporary progress shows that networks inspired by realistic neuronal populations and trained by *learning algorithms* can reach the theoretical limits for optimal decoding performance (Hillar & Tran, 2018; Gallager, 1968). The actual learning procedures for spiking neural networks and the analysis of their performance and of their biological relevance are an active area of research in the field of neural coding (Maass, 1997; Kostal & Kobayashi, 2019; Stöckl & Maass, 2021; Zenke et al., 2021).

[1] The situation is not unlike the famous case of George Gemow's "Diamond code" hypothesis which sought to explain the information carried by the DNA molecule shortly after its discovery by Watson and Crick. While the code was optimal from the mathematical perspective, it later turned out to be wrong due to biological constraints which make its use impossible. The fundamental idea, which is that the nucleobases are arranged into amino-acid encoding triplets was however right and it initiated further research in the field.

Although we cannot claim that the code which turned out to be the most reliable is the most likely to be true, the information obtained from the analysis provides us with critical insight and can eventually reveal the code being used.

Based on the temporal resolution, neural coding hypotheses are generally divided into two types, the *frequency code* hypothesis, and the *temporal code* hypothesis. Both will be described in detail in the following text. We should however note beforehand that the dividing line between the two types is not sharp, and they rather continuously transform into one another.

2.2.1. Frequency code hypothesis

The frequency code (also denoted as the *rate code*) is the historically oldest way to interpret spike trains (Adrian & Zotterman, 1926). According to this concept, the only aspect of spike trains that contains information is the firing rate, i.e., the number of spikes per unit time. The fact that the precise timing sequence of spikes generated by a given stimulus often varies from trial to trial is ignored by this code and the inter-trial timing irregularities are considered to be just uninformative noise (Stein et al., 2005). Therefore, if the total number of spikes within a certain time interval does not differ among trials, the neural representation of a stimulus within this interval is identical. The exact length of such an interval is not predefined and the experimentalist is free to adjust it to the specific conditions and intentions (Gerstner & Kistler, 2002). However, if the experimentalist's intention is to determine the "pure" rate code, the interval should be set sufficiently long otherwise the encoded information would be affected by spike timing and the code would be therefore partially temporal. What is commonly considered sufficient are intervals 50 to 500 ms long but the number can differ significantly for hypo- and hyperactive neurons and for different stimulus time scales (Borst & Theunissen, 1999; Dayan & Abbott, 2005; Kostal & Kobayashi, 2019; Perkel & Bullock, 1968). The experimentalist can also manipulate the placement of the time windows. Thus, the calculation of neuronal firing rate can give us different results depending on the specific combination of adjustable parameters (length and placement of the time windows).

There are other ways to estimate the neuronal firing rate, which do not operate with discrete time intervals as described above. Essentially, spikes are substituted with "kernels" (Gaussian, exponential, or other basic curves), which are then summed into a smooth firing rate curve. However, even these methods are not spared of some level of arbitrariness as they too operate with a number of adjustable parameters. This topic will be further discussed in detail in section 4.2.2.

Despite that the rate code can be, due to omitting stochasticity in spike timing, quite robust, it has been repeatedly criticized for its questionable viability within neural systems. It is opposed mainly by the fact that reaction times in behavioral experiments are often so short that they don't allow for long-enough time periods that the rate code requires for stimulus evaluation. To demonstrate on an example, humans can recognize and respond to visual scenes in less than 400 ms (Thorpe, Fize & Marlot, 1996). The process is realized by several consecutive neurons and if each of them would have to wait and perform a temporal average in order to read the message of the presynaptic neuron, the actual reaction time would be much longer.

Even though the coding precision can be relatively low on the level of first-order neurons, the convergence of many first-order neurons to fewer second-order neurons can result in a relatively accurate and robust code. For example, the first two layers of the moth olfactory system are organized in such a way that the first-layer neurons (ORNs) converge onto a much smaller number of second-layer (antennal lobe) neurons (Hansson, 1995). The signal-to-noise ratio of the pooled signal increases with the square root of the number of ORNs (Rospars et al., 2014; Kostal & Lansky, 2013). Information theory then predicts that the optimal ORN tuning curve (the dependence of the response firing rate on the stimulus intensity) should match the profile of the stimulus distribution in a certain way (see Kostal, Lansky & McDonnell, 2013 for details). Such relationship has been recently indeed verified also in the experimental data (Levakova et al., 2018).

2.2.2. Temporal code hypothesis

Temporal code is a code that stores information in precise spike timing. It offers an alternate explanation to the observed irregularity of spike occurrence within spike trains, claiming that it is not noise, as the rate code would suggest, but rather a meaningful way in which neurons encode information.

Let us illustrate the difference on an example. Suppose we are given a 12 ms long spike train that contains 6 spikes. The spike train is divided into 1 ms intervals marked by 1 or 0 depending on whether they contain a spike. Now imagine two such spike trains, one represented by the series *000111000111* and the other by *001100110011*. We can see that even though their firing rate is the same (500 Hz), and so in the context of rate code they both have the same meaning, in the temporal coding scheme their meaning is different (Theunissen & Miller, 1995).

However, not all spikes and their precise timing are necessarily relevant. There are several temporal coding hypotheses differing in the various aspects of spike trains that are taken into account and some of the hypotheses only concern spikes that meet certain criteria.

Time-to-first spike hypothesis states that information is encoded in the delay between the stimulus onset and the firing of the first spike. This scheme requires the existence of an internal reference point that marks the stimulus onset. As for vision, information about the onset of a saccade could serve this function (Kupper et al., 2005). A neuron that fires shortly after the reference signal could signal a strong stimulation, firing somewhat later would signal a weaker stimulation. One of the advocates of this code is S. Thorpe who argues that the brain does not have time to evaluate more than one spike from each neuron per processing step and therefore the first spike should contain most of the relevant information (Thorpe et al., 1996).

Some sort of time reference is however a general requirement for all temporal codes (Stein et al., 2005). Since there is no absolute time reference in the nervous system (neurons do not have a sense of "absolute" time, let alone in the millisecond scale)

relative reference signal has to be employed. In the previous example, it is a single event, the time of a saccade realization, but the signal can also be periodic.

Phase-of-firing hypothesis states that neurons orient themselves in time by using neural oscillations, or brainwaves as the reference scheme. Brainwaves are quite common in the hippocampus, in the olfactory system, as well as in other areas of the central nervous system. Neuronal spike trains could therefore encode information in the phase of spikes with respect to the background oscillation. For example, according to the findings of O'Keefe (1993), the phase of a spike during an oscillation in the hippocampus of the rat conveys information on the spatial location of the animal which is not fully accounted for by the firing rate of the neuron. The assumed mechanism of the phase-of-firing code is that spikes occurring at specific phases of an oscillatory cycle are more effective in depolarizing the post-synaptic neuron.

Inter-spike interval (ISI) hypothesis: Another possible reference signal can be the spike train itself. In this case, the time of a certain spike is related to the time of the previous spike, in other words, information is encoded as the time between successive spikes. The hypothesis is based on the fact that the likelihood of a spike depolarizing the post-synaptic neuron increases with the number and proximity of previous spikes within the spike train. The two series from the second paragraph of subsection 2.2.2. - *000111000111* and *001100110011* could for example result in two post-synaptic spikes, or zero post-synaptic spikes respectively, in case at least three spikes in a row would be necessary to evoke an action potential.

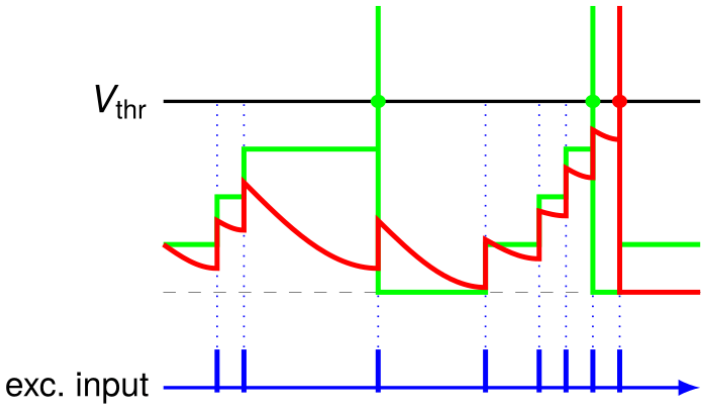

Figure 3: The postsynaptic activity of a simplified neuronal model depends on the precise timing of presynaptic spikes. Presynaptic excitatory spikes (blue) depolarize the postsynaptic membrane towards the threshold of excitation. Assuming the postsynaptic membrane acts as an ideal capacitor (green) implies that only the total number of input spikes matters (pure rate code). However, the leakage current typically drives the membrane voltage back to its resting state (red), and therefore only certain inputs, with spikes sufficiently close together, lead to postsynaptic spiking activity (temporal code).

2.3. Efficient coding hypothesis

Unlike the neural coding hypotheses that we have discussed so far, the *efficient coding hypothesis* does not seek to specify the exact way how information is communicated between neurons. Rather it is concerned with the optimality of this communication. The hypothesis is a generalized form of the original Horace Barlow's redundancy-reducing theory (Barlow, 1961). It states that neural systems are adapted, by evolutionary and developmental processes, to the natural statistical structure of sensory signals. Their adaptation leads to the optimization of stimulus encoding in these systems. In what way is the encoding optimized is not defined by the hypothesis. Therefore, the optimization criterion has to be chosen and examined by the researcher.

The efficient coding hypothesis has been studied extensively across different sensory systems and animal species. Most studies focus on the visual system (Atick, 1992; Bialek & Owen, 1990; Hateren, 1992; Hornstein et al., 2000; Laughlin, 1981; Laughlin, 1996).[2] and on the auditory system (Lewicki, 2002; Smith & Lewicki, 2006; Watkins &

[2] The problematic is summarized in the review by Simoncelli and Olshausen (2001).

Barbour, 2008), including the auditory system of insects (Machens et al., 2005). The olfactory system is studied to a much lesser extent. One of the main reasons why the olfaction has been relatively neglected lies in the technical difficulties in measuring and controlling the stimulus delivery. For example, the statistics of odorants encountered by moths in their natural environment have so far been impossible to obtain experimentally (Murlis, Willis & Cardé 2000) and it is difficult to reproduce these statistics in the laboratory setting (Gorur-Shandilya et al., 2017). On the other hand, theoretical statistical predictions of the main stimulus characteristics are available (Celani, Villermaux & Vergassola, 2014), and have been implemented in both experimental (Jacob et al., 2017) and theoretical (Levakova et al., 2018) studies to simulate the natural conditions. In summary, the investigation of the efficient coding hypothesis in case of insect olfaction remains an underrepresented and challenging area of current computational neuroscience research.

2.3.1. The impact of stimulus statistics on neural coding efficiency

In order to illustrate the tight relationship between the stimulus statistics and the optimal neuronal coding strategy, we first briefly review a classical study done by Simon Laughlin which states that sensory neurons are adapted in such a way so that the entropy of their response is maximized (Laughlin, 1981). More generally, sensory neurons are hypothesized to maximize the *mutual information* between stimuli and responses, while the response entropy maximization holds within the hypothesis under specific conditions (Kostal, Lansky & McDonnell, 2013). Nonetheless, the adaptation, resp. optimization is based on natural stimulus statistics, which means it is of great importance whether the stimulus intensity (or another stimulus parameter) is common or rare.

According to Laughlin, for a simple case of a receptor neuron whose response variability is small and independent of the stimulus, it holds that the intensity-response function describing neural response corresponds to the cumulative probability function of stimulus intensities (Fig. 4). If a neurons' response range would not be limited (mainly by the refractory period), there would be no reason for this to be true. The input

intensities are however transferred into a compressed range which does not allow neurons to assign a unique code to every intensity value. In order to cover all possible stimulus intensities, neurons have to lose some information by reducing the resolution in which they discriminate differing intensities. It is up to evolution to optimally set the sensitivity of sensory neurons. If sensitivity is set too high then inputs will often saturate the response, and information about high-intensity inputs will be lost. On the other hand, when sensitivity is set too low, large parts of the response range are underutilized because they are reserved for exceptionally large excursions of input. In summary, the setting of the receptor neuron sensitivity determines its ability to discriminate a particular stimulus intensity. On the intensity-response curve, the resolution or discriminability is represented by the slope of the curve.

Now, let us circle back to the statement in the first paragraph of the chapter, which is that the entropy of the neural response should be maximized. According to this statement, if we divide a neuron's response range into discrete levels, all of them should be used with equal frequency. It follows that every response level should cover such a range of intensities so that the area under the stimulus' distribution curve would be the same for all the response levels. This coding scheme favors inputs with high expected frequency and provides them with greater resolution while, on the other hand, keeping the resolution of improbable events low.

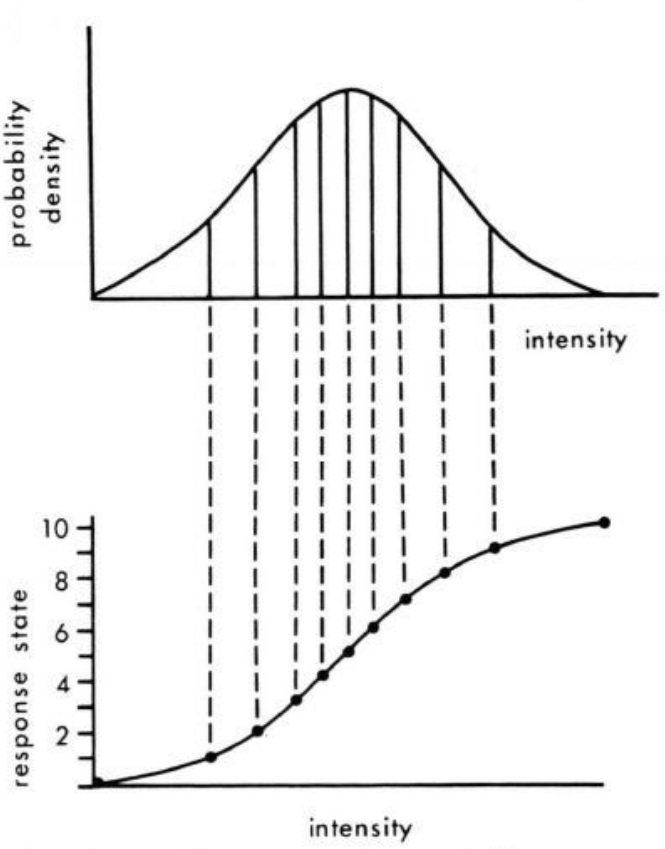

Figure 4: Optimal allocation of neuronal response states for a given probability density of stimulus intensities (top). The amount of transferred information is limited by the finite range of possible response states (bottom). Due to the nonlinearity of the stimulus-response curve, each response state encodes different relative changes in stimulus intensity. Maximum information is transferred if all response states are used equally, i.e., if the area under the stimulus pdf is equal for each response state. In other words, the optimal stimulus cumulative distribution function corresponds to the (normalized) stimulus-response function (Adapted from Laughlin (1981)).

The classical one-dimensional result of Laughlin (1981) can be generalized and re-interpreted to hold not only for the global distribution of stimulus intensities but also to account for local changes of the distribution or even for the temporal dynamics of the stimulus. The limited neural coding range often does not cover the whole range of possible stimuli values (Dean, Harper & McAlpine, 2005; Wen et al., 2009; Durant et al., 2007) and the efficient coding hypothesis predicts that neurons transiently adapt their coding strategies to match the local stimulus distribution (Wark, Lundstrom & Fairhall, 2007). In particular, the response reliability increases near the most commonly occurring stimuli in order to minimize the overall decoding error and to maintain the

efficient representation of the environment. Such situation is reported in the auditory coding of the sound intensity (Dean, Harper & McAlpine, 2005; Watkins & Barbour, 2008; Wen et al., 2009; Watkins & Barbour, 2011), of the interaural level differences (Dahmen et al., 2010) and time differences (Maier et al., 2012), but also in the neural coding in the primary visual cortex (Durant et al., 2007) and primary somatosensory cortex (Garcia-Lazaro et al., 2007). Furthermore, it has been shown recently that the responses of olfactory receptor neurons follow the statistics of fluctuation timescales in odor plumes so that pheromone encounters are encoded best after the most frequent durations of blanks (i.e., time zones with no pheromone present) and that the average coding accuracy is adjusted to the stimulus statistics at a particular distance from the odorant source (Levakova et al., 2018)).

These recent results thus provide inspiration for the task investigated in this thesis. In particular, we investigate whether – and in which sense quantitatively – is the ORN response more reliable for the natural-like fluctuating stimulation, when compared to the artificial constant single-pulse pheromone dose.

2.4. Pheromone reception in *Lepidoptera*

2.4.1. Character of natural pheromone stimulation

Orientation towards food, and especially towards mate in insects, is an olfactory-controlled behavior that relies on the detection of odorant or pheromone molecules, respectively, delivered from the source. The atmospheric turbulence causes strong mixing of air and creates a wide spectrum of spatio-temporal variations in the time-course of the concentration signal (Jones, 1983; Murlis, 1996). The mean concentration of pheromone decreases monotonically with the distance from the source, however, the relation for concentration fluctuations and thus for the instantaneous magnitude of the signal is more complicated (Celani et al., 2014).

Due to the inhomogeneous mixing, very high concentration values can be found in a wide range of distances from the source, though their frequency decreases with distance

(Jones, 1983). An important characteristic of the detected signal is its intermittency, i.e., the fraction of time during which non-zero concentrations are detected. It has been shown that the natural signal is highly intermittent (Mylne & Mason, 1991; Murlis et al., 2000). The signal is present less than 50 % of the total time, and usually, even smaller intermittency is detected, e.g., Murlis et al. (2000) report 20 % in measurements of pheromone dispersion in natural conditions close to the source. Various types of ion detectors are usually employed for measurements, though Baker and Haynes (1989) and Murlis et al. (2000) have also used electroantennogram responses.

The variations in the concentration of the pheromone are essential for the insect to locate the source of the stimulus. The animal loses direction to the source and its upwind flight gets "arrested" if it gets into a cloud of homogeneously distributed pheromone (Kennedy et al., 1980; Willis & Baker, 1984). Experiments in tunnels have shown that characteristics like frequency and intensity of the intermittent stimulus play a key role in maintaining the proper direction of flight (Vickers & Baker, 1992). The insect's sensory system differs from the ion detector and thus the level of temporal and spatial detail the receptor neuron perceives is limited by both physical and biochemical reasons (Baker & Haynes, 1989; Kaissling, 2001).

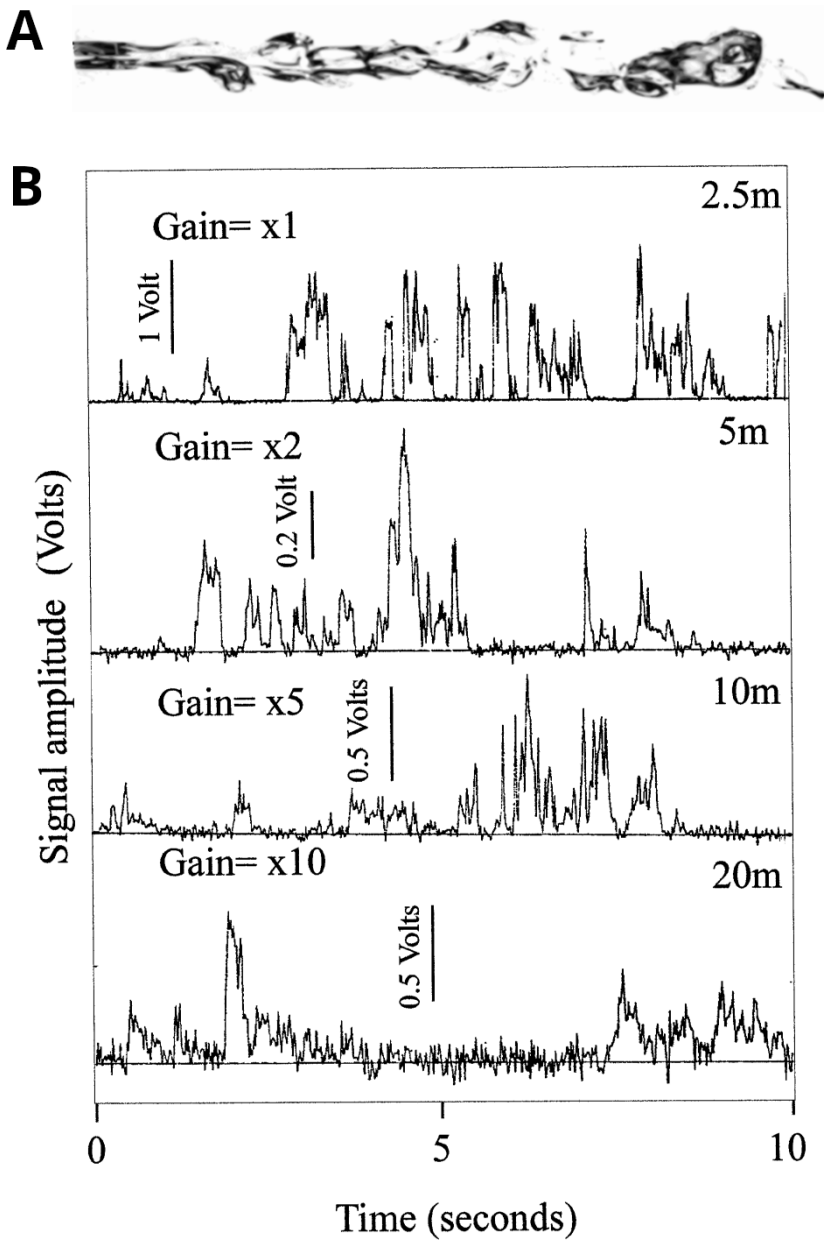

Figure 5: Properties of natural pheromone stimulation. (A) Visualization of a pheromone plume, extracted and adapted from a digitized image of a smoke plume substitute filmed in a wind tunnel 1 m across and 2 m long with source on the left side (With permission from Belanger and Willis (1998).). Due to non-homogeneous (turbulent) airflow, high pheromone concentrations occur at far distances from the source. (B) Experimentally measured fluctuations in the concentration of substitute tracers (as the real pheromone cannot be assured by ion detectors) at different distances from the source. The result is a highly intermittent signal in time, consisting of short pulses of relatively undiluted and concentrated signal. (Adapted from Kostal, Lansky, and Rospars (2008), Murlis, Willis, and Cardé (2000).).

2.4.2. Architecture of olfactory sensilla

The smell is a crucial sense for many insects. Recognition of volatile chemical compounds and their ratios signalizes the presence of food sources, oviposition sites, predators, mates, and other conspecifics in the area. Olfactory receptor neurons (ORNs) are cells devoted to the detection and recognition of chemical compounds. They are located within insect's antennae, more specifically beneath sensilla, hair-like structures extending from their surface (Steinbrecht, 1997). There are two types of olfactory sensilla - short *sensilla basiconica*, which detect general odorants, and long *sensilla trichodea*, which are pheromone-sensitive and the ORNs they host are therefore also referred to as the pheromone receptor neurons (PRNs). Apart from olfactory sensilla, there are also antennal sensilla of other modalities.

Sensilla trichodea form regular brush-like arrays on each annulus of the antennal flagellum and are the most abundant antennal sensilla (constituting about 38% of 2100 sensilla per annulus in *Manduca sexta*) (Keil, 1989; Lee & Strausfeld, 1990). Each *sensillum trichodeum* is typically innervated by two ORNs (Kaissling et al., 1989; Kaissling et al., 1978). One ORN responds to the main sex pheromone component and the other one to other components of the pheromone blend. Apart from ORNs, each sensillum contains three additional non-excitable cells: the trichogen cell, the tormogen cell, and the thecogen cell. The thecogen cell wraps around ORNs. It covers their whole somata and a part of their dendrites, the so-called inner dendrites. The naked outer dendrites extend into the hair lumen filled with aqueous lymph and the pheromone receptors (PRs) are located on their surface. The somata and the inner dendrites are embedded between epithelial cells underneath the hair. Axons are covered by glial sheets and project to the antennal lobe of the brain (Ai & Kanzaki, 2004; Anton & Homberg, 1999; Hansson & Christensen, 1999). The cuticle of the hair is penetrated by 10 nm wide pore tubules extending into the hair lumen (Steinbrecht, 1997) through which pheromone molecules enter. Because pheromone molecules are hydrophobic and as such don't dissolve in the aqueous lymph, to get to the surface of outer dendrites and bind to PRs, they need to be transported by carrier proteins called the pheromone-

binding proteins (PBPs) that are present in the lymph (Vogt & Riddiford, 1981). PBPs (and OBPs in general) contribute to the specificity of pheromone detection as there are different PBP types tuned to defined, partially overlapping sets of ligands (Forstner et al., 2009; Guo et al., 2012).

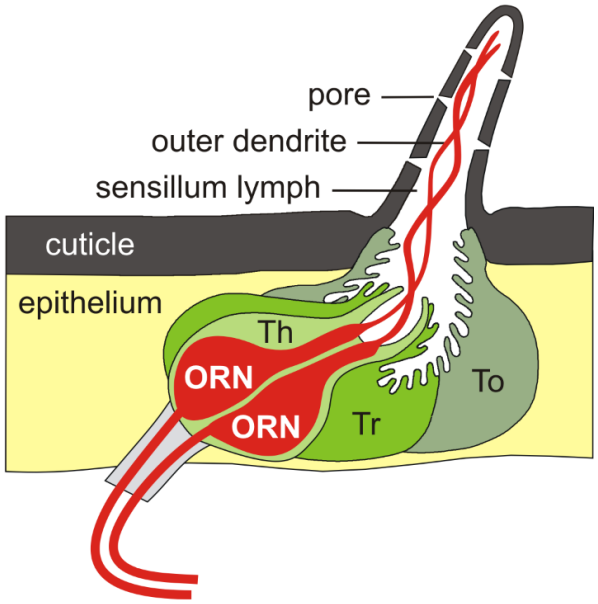

Figure 6: The sensillum on the moth antenna. The olfactory receptor neuron (ORN) is located inside a hair-like structure (the sensillum). The pores in the cuticle allow the entry of odorant (pheromone) from the surrounding air into the sensillar lymph, where it binds to the specific receptors on the dendrites. One sensillum can contain more than one ORN. The soma of the neuron is surrounded by the three auxiliary cells (thecogen Th, trichogen Tr and tormogen To).

2.4.3. Fate of pheromone molecules inside sensilla

A pheromone molecule destined to activate its respective receptor must undergo a series of processes, the first one being its absorption onto a *sensillum trichodeum*. From the air making direct contact with the surface of antennae, 80% of pheromone molecules get adsorbed onto *sensilla trichodea* (Kanaujia & Kaissling, 1985). Next, the molecule has to migrate from the adsorption site to a pore and from there to the inner end of the pore tubule. Given that the distance between pores and the thickness of the hair wall are both only 0.5 micrometers or less, the expected mean time between adsorption and arrival to the inner end of a pore tubule is in the millisecond range. When at the inner end of a pore tubule, the pheromone molecule binds to the PBP. The pheromone-

PBP complex then diffuses over a distance of about 1 micrometer to the surface of the outer dendrites, which accounts for a further delay of about one ms.

The concentration of the PBP in the lymph is around 10 mM, therefore extremely high (Klein, 1987). In a single sensillum, several PBP species with different binding specificities can be present (Forstner et al., 2009; Guo et al., 2012; Maida et al., 2003). Sex pheromones of *Antheraea polyphemus* and *A. pernyi* are both composed of three different components. In the sensilla trichodea of these species, there are three types of PRNs as well as three types of PBPs and each PBP preferentially binds one of the three pheromone components (Maida et al., 2003).

The PBP molecule folds up into a sphere that has a hydrophilic outer surface and hydrophobic central cavity which can accommodate a pheromone molecule. At a given moment, a PBP molecule is either in closed or opened conformation depending on the local pH. When pH is low, the internal binding cavity is expanded and a lid connecting it with the surroundings opens, in this conformation, a pheromone molecule can enter or exit the cavity. This corresponds with the fact that the cell membrane and the pore tubule inner surface are negatively charged and that therefore, the pH is low near these sites. When a pheromone molecule enters the sensillum through a pore tubule, it encounters an opened PBP molecule into which it can bind. The binding induces a conformational change that encloses the pheromone molecule inside the PBP. When the pheromone-PBP complex arrives at the cell membrane, it opens and releases the ligand which is now free to bind to the receptor. The majority of pheromone molecules, 83% to be precise, really bind to the PBP after entering the lumen. 17% of pheromone molecules however first encounter a molecule of a degrading enzyme instead of a PBP molecule and get rapidly degraded (K.-E. Kaissling, 2009). The rest of the pheromone molecules bound to the PBP is however protected from degrading enzymes to a great extent and their degradation proceeds 20,000-fold more slowly. Without the PBP, 97% of the pheromone would be degraded before binding to the receptor (K.-E. Kaissling, 2009) and the half-life of the pheromone would be 13 ms (Ishida & Leal, 2005) or 15 ms (Vogt et al., 1985), in contrast to the 4.5 minutes found by Kasang et al. This slow

degradation contrasts with the fast receptor potential decline (K.-E. Kaissling, 2009). To explain the discrepancy, stimulus deactivation was postulated. It is thought that the pheromone-PBP complex in the closed conformation undergoes a structural change that blocks the transition to the opened conformation. It is believed that what triggers this conformational change is an alteration in the hydrophobic C-terminal tail. It was confirmed by experiments that both complete removal of the C-terminal tail (Leal et al., 2005; Michel et al., 2011) and a one-point mutation of the C-terminal tail (Xu & Leal, 2008) disables transition to the opened conformation and the pheromone gets irreversibly locked inside the central cavity. Because after strong stimuli, the neural response declines more slowly than after weak stimuli (K.-E. Kaissling, 1974), it is presumed that the deactivation process is saturable. All these informations point to the existence of an enzyme that deactivates the pheromone-PBP complex by binding to and blocking, removing, or altering its C-terminus tail. When a pheromone molecule successfully arrives to the plasma membrane of an outer dendrite without being degraded or deactivated, it gets exposed and interacts with the receptor molecule while still bound to the PBP (K.-E. Kaissling, 2009). Binding of pheromone to the receptor however requires another additional protein and that is the sensory neuron membrane protein (SNMP1). The SNMP1 is located in close proximity to the receptor in the membrane and functions as a co-receptor that helps in docking the pheromone-PBP complex at the receptor molecule (Benton et al., 2007; German et al., 2013).

2.4.4. Pheromone receptors and associated signal transduction pathways

The odorant receptors (ORs) are a family of receptors that recognize diverse odorant molecules present in insects' environment. The PRs (pheromone receptors) are a subset of the ORs responsible for the detection of pheromone molecules. The ORs, as well as the G-protein coupled receptors (GPCRs), possess seven transmembrane domains. However, ORs and GPCRs are not related as they lack sequence similarity and have different topologies. (ORs have intracellular N-terminus and extracellular C-terminus as opposed to GPCRs which have extracellular N-terminus and intracellular C-

terminus.) (Benton et al., 2006; Lundin et al., 2007; Smart et al., 2008) ORs are expressed in ORNs (olfactory receptor neurons). Single ORN usually expresses only one type of OR (Dobritsa et al., 2003; Hallem et al., 2004), however, exceptions to this rule have been found. The number of ORNs expressing a specific OR type correlates with the ecological importance of the respective chemical compound that the OR type detects. For example, in male *Bombyx mori*, the OR type BmOR1 which binds the major sex-pheromone component *bambykol* is expressed in an extremely large subset of ORNs (Krieger et al., 2005; Sakurai et al., 2015).

The family of ORs includes a unique member called Orco (Vosshall & Hansson, 2011). Its name is derived from its role as the general OR coreceptor, which means it forms heteromeric complexes with all the other OR proteins. Therefore, it is expressed in all OR-expressing ORNs (Larsson et al., 2004; Vosshall et al., 1999). It shares only low sequence identity with other ORs but is highly conserved across insect species and even orders (Jones et al., 2005; Krieger et al., 2003). When in the cytoplasm, it associates with unstable OR molecules and protects them from degradation. After the complex is formed, Orco stabilizes the associated OR molecule and targets it to the cell membrane (Benton et al., 2006). Orco can however localize itself into the dendritic membrane even in the absence of ORs and form a functional cation channel.

The ligand specificity of an OR/Orco complex is determined solely by the respective OR type. OR can recognize either several different chemical compounds or, in case of pheromones, just one. The high specificity of PRs reflects the vital importance of the pheromone signal. Whether Orco participates in the receptor signaling and whether the signaling is ionotropic or metabotropic is not yet clear. Some studies provide evidence that Orco and OR together form an odor-gated cation channel that carries out ionotropic signal transduction (Nichols et al., 2011; Sato et al., 2008). Other studies follow up with findings that the receptor complex functions not only as a cation channel but also as a metabotropic G protein-coupled receptor. (Deng et al., 2011; Wicher et al., 2008). On the basis of these findings, the model of dual activation has been proposed which states that the primary response is generated by activation of ligand-gated ion

channels, followed by a G-protein-mediated potentiation or modulation of the ionotropic response (Nakagawa & Vosshall, 2009). Recent studies on *Manduca sexta* however haven't provided any evidence for PR/Orco-based ionotropic pheromone transduction and hypothesized that the signal transduction may be exclusively metabotropic (Nolte et al., 2013, 2016). On top of that, it was found that Orco constitutes not only the OR/Orco complex but also by itself forms a spontaneously opening cation channel regulatable by ligand-binding. Based on these findings, it has been proposed that Orco serves as a voltage-gated and second-messenger gated pacemaker channel, controlling the membrane potential and thus the threshold and kinetics of the pheromone response.

It is hypothesized that the second messenger of the PR/Orco complex is inositol trisphosphate (IP3). This hypothesis is supported by a number of evidence. Pheromone stimulation of antennal tissues elicits the formation of IP3 (Boekhoff et al., 1990). Upon exposure to pheromones, three electrical currents in cultured moth ORNs are reported. A first and very rapid Ca2+ current that declines within several milliseconds. A second and slower current that declines within 3s and a third and sustained inward current that lasts over several seconds and is Ca2+ independent. Perfusion of cultured moth ORNs with IP3 elicits a similar sequence of inward currents that strongly resemble pheromone-evoked currents (Stengl, 1993, 1994; Stengl et al., 1992). Similarities indicate that pheromones activate a metabotropic signaling pathway mediated by PLCβ, leading to an enhanced formation of IP3 and DAG. Activation of IP3-gated Ca2+ channels in the membrane of ORNs leads to a rise in Ca2+ that rapidly opens Ca2+-activated cation channels. DAG might enhance PKC activity, thus eliciting the third pheromone-evoked inward current (Stengl, 2010; Stengl & Funk, 2013). It is a matter of debate whether a metabotropic pheromone transduction process that includes a series of enzyme-catalyzed reactions is fast enough for the required physiological responses. However, the example of phototransduction indicates that a G protein-mediated reaction cascade could be indeed fast enough for a rapid response to pheromone signals.

3. Overview and Aims of the Thesis

The aim of our study is to verify the efficient coding hypothesis in the context of the insect olfactory system. We specifically focus on the moth pheromone receptor neurons and the temporal dynamics of the pheromone stimulation. As the adaptation criterion (see chapter 2.3.) we choose the spiking response reproducibility and reliability, which we evaluate with the use of several quantitative descriptors. We ask whether a natural-like stimulation pattern can lead to a more reliable neural response than an artificial square pulse stimulation. To find the answer, we have obtained experimental data from the collaborating laboratory (dr. Lucas, INRAe, Versailles, France) and examined the neural response reproducibility by using both classical (Perkel, Gerstein & Moore,1967a; Perkel, Gerstein & Moore, 1967b; Dayan & Abbott, 2001) and recently proposed statistical methods (Shinomoto, Shima & Tanji, 2003; Kostal, Lansky & Pokora, 2013; Kostal, Lansky & Stiber, 2018).

Inspiration: In a classical paper, Bryant and Segundo (1976) report that the spiking response of the *Aplysia* abdominal ganglion neurons is remarkably invariant when exposed to repeated stimulation with a rapidly fluctuating current. The authors conclude that spikes are generated with greater reliability if the membrane potential at the spike initiation zone changes rapidly, with the spike timing locked to certain trajectory shapes of intracellularly injected current. The exact biophysical mechanisms responsible for this effect were, however, not identified. The outstandingly high spiking precision was illustrated in a follow-up work (Mainen & Sejnowski, 1995) using the occipital cortical neurons of the rat, contrasting the difference in responses over repeated stimulation with either constant or fluctuating current (Fig. 7). The authors speculate that the sodium channel inactivation might be responsible for a rapid increase of spiking probability during sufficiently fast hyperpolarizing input event. The problem of response reliability to a dynamic stimulation has been further investigated for various neuronal types in multiple follow-up studies (e.g., see Ruyter van Steveninck et al., 1997; Berry, Warland & Meister, 1997; Cecchi et al., 2000 and references therein). The

reported findings are however not conclusive with some studies demonstrating higher response reliability for a static rather than dynamic stimulation. For example, Warzecha and Egelhaaf (1999) study the H1 neurons in the fly visual system and argue that the previously described high precision for the fluctuating case is largely due to data misinterpretation.

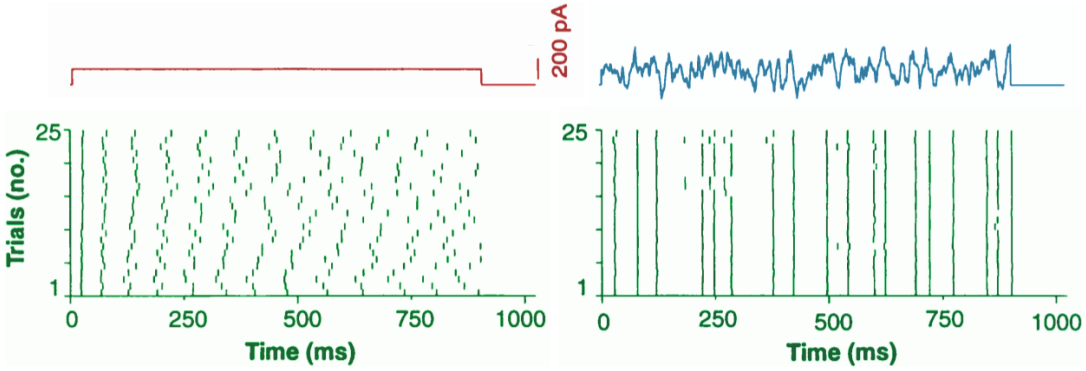

Figure 7: Spiking responses (green) of rat cortical neurons over 25 repeated trials, exposed either to the constant (red) or fluctuating (blue) injected current. Note the remarkably high response invariance to the fluctuating stimulation. (Adapted from Mainen and Sejnowski (1995).)

The main goal of this thesis is to contribute to the unresolved debate by investigating a different neuronal system (insect pheromone reception), which has not been studied before within the context of response reliability. We use experimental data from a novel stimulation device (olfactometer) from the collaborating laboratory of Dr. P. Lucas, INRAe, Versailles, France). The new type of olfactometer overcomes certain well-known fundamental technical issues related to the precision of the stimulus (pheromone) delivery (Barta et al., 2022). Furthermore, we interpret our results in the context of the efficient coding hypothesis. These two aspects (the insect olfactory system plus the efficient coding hypothesis) together with the application of recently proposed rate and temporal coding analysis methods (Kostal, Lansky & Pokora, 2013; Kostal, Lansky & Stiber, 2018) represent the main scientific novelties of this thesis.

Expectations: According to the efficient coding hypothesis, as explained in the previous sections, the neural response is adapted to the stimulation characteristics encountered by the organism in its natural environment. Furthermore, the natural time-course of the pheromone concentration is highly *intermittent* and dynamic (Murlis,

1996; Kostal, Lansky & Rospars, 2008; Celani, Villermaux & Vergassola, 2014), consisting of relatively short stimulation pulses (whiffs) separated by pauses with zero pheromone concentration (blanks), see Fig. 5. We, therefore, expect that the olfactory receptor neurons are better adapted to encode the natural-like (fluctuating) stimulus rather than the artificial one (constant pheromone pulse of 2s duration). We do not *a priori* assume the exact form of this adaptation as the previously published conflicting results on a different sensory modality (Warzecha & Egelhaaf, 1999; Ruyter van Steveninck et al., 1997) show that a careful approach is needed when interpreting the observed data. Hence, we use a battery of methods, both classical and recently proposed, in order to identify the nuances in the responses either for the whole population or for individual neurons. Unlike previous studies, we examine the data assuming both rate and temporal coding hypotheses.

4. Methods

4.1. Experiment

All the data that we worked with were obtained by experiments that took place in the laboratories of the Department of Sensory Ecology, INRAe, Versailles, France.

The experiments were performed on 4 to 5 days old, sexually mature males of *Agrotis ipsilon*. The males were separated from the females during the pupal stage and then kept in separate rooms to ensure that they would later be naïve to the female sex pheromone. Because *Agrotis ipsilon* is a nocturnal species, both sexes were kept under an inversed light-dark cycle, so that technicians could perform the experiments during the objective day (in red light).

The moth was fastened between two pieces of Styrofoam with only his head protruding. One of the antennae was secured by tape to another piece of Styrofoam (Fig. 8). The Styrofoam holder also comprised a magnet that would firmly fix it onto the magnetic table. The moth was then placed under the stereomicroscope so that the experimentalist could control the insertion of electrodes. With the use of the micromanipulator, the recording electrode was carefully inserted into the base of a long pheromone-responding *sensillum trichodeum*, the referential electrode was inserted into the insect's eye. The electrodes used were the tungsten electrodes (TW5-6; Science Products, Hofheim, Germany). The major sex pheromone of *A. ipsilon*, (Z)-7-dodecenyl acetate (Z7-12:Ac) was loaded on a 10 × 2 mm filter paper and delivered through a calibrated capillary (ref. 11762313; Fisher Scientific, France) into which the paper was inserted. The delivery was controlled by an electrovalve (LHDA-1233215-H; Lee Company, France).

One sensillum was recorded per insect. The electric signal was amplified (×1000) and band-pass filtered (10 Hz to 5 kHz) with an ELC-03X (NPI electronic, Tamm, Germany), and sampled at 10 kHz by a 16-bit acquisition board (NI-9215; National Inst., Nanterre, France) under Labview (National Inst.).

The stimulation protocol was designed as follows (see Fig. 9). There were two types of the pheromone concentration delivery time-course (also denoted as 'patterns'): the *fluctuating* and the *constant* type. The constant type was a 2s long pheromone pulse of invariable concentration. The fluctuating type was also 2s long, consisting of a sequence of short pulses (whiffs) interrupted by pauses (blanks). The pheromone concentration was the same for all whiffs and the time-course of the fluctuating pattern was fixed and selected before the experiment, therefore each neuron was exposed to exactly the same stimulus dynamics. The stimulation intervals of the two types were alternated and always separated by a 30s long pause. The particular duration values (2s, 30s) were chosen with respect to the fact that the moth can endure the recording only for a limited period of time (ca. 20 min). Therefore, a compromise has to be made to at least partially satisfy the following conditions.

1) The stimulation patterns must be sufficiently long.

2) The stimulation intervals must be separated by sufficiently long pauses so that the sensory adaptation is suppressed.

3) A sufficient number of trials must be obtained for each stimulation type.

The pheromone dose in the constant case was 10pg, in the fluctuating case the dose was twofold, i.e., 20pg so that the same average number of spikes would be obtained for both types of stimulation. This way, the responses could be compared meaningfully. (Note that the actual pheromone concentration near the sensillum cannot be measured and is potentially affected by the constant vs. intermittent airflow, hence the two different pheromone doses.) However, calibration experiments with non-pheromone odorants confirm high temporal precision and steadiness of the delivery (Barta et al., 2022)).

The records were then processed by semi-automatic spike sorting. Ultimately, 78 spike trains have been obtained.

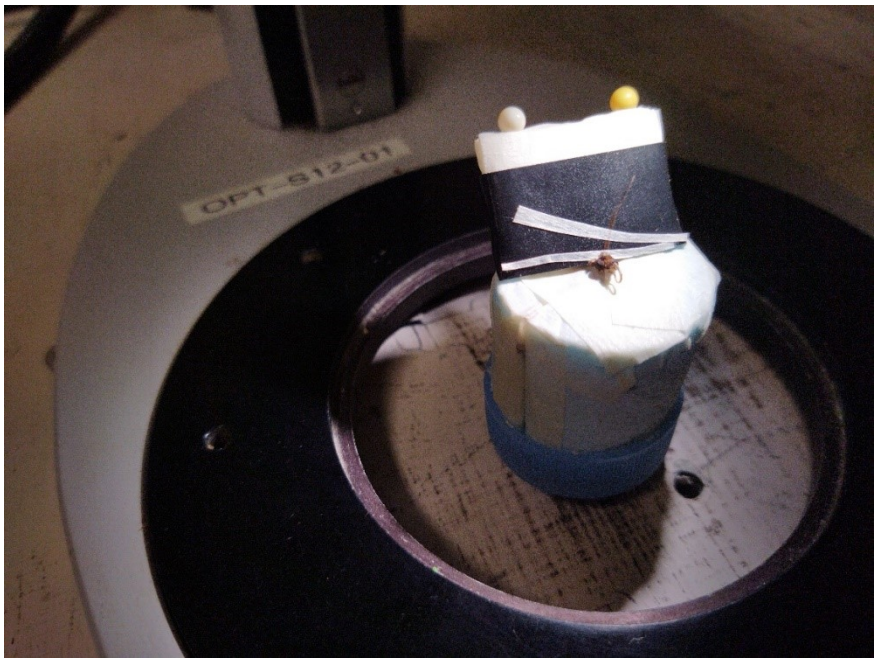

Figure 8: A live male individual of *A. ipsilon* is immobilized and ready to be recorded. One of its antennae is fixed onto a piece of Styrofoam. The recording electrode will be inserted between the two strips of tape, into the base of a long *sensillum trichodeum*. (Own photography, taken with the permission of Dr. P. Lucas.)

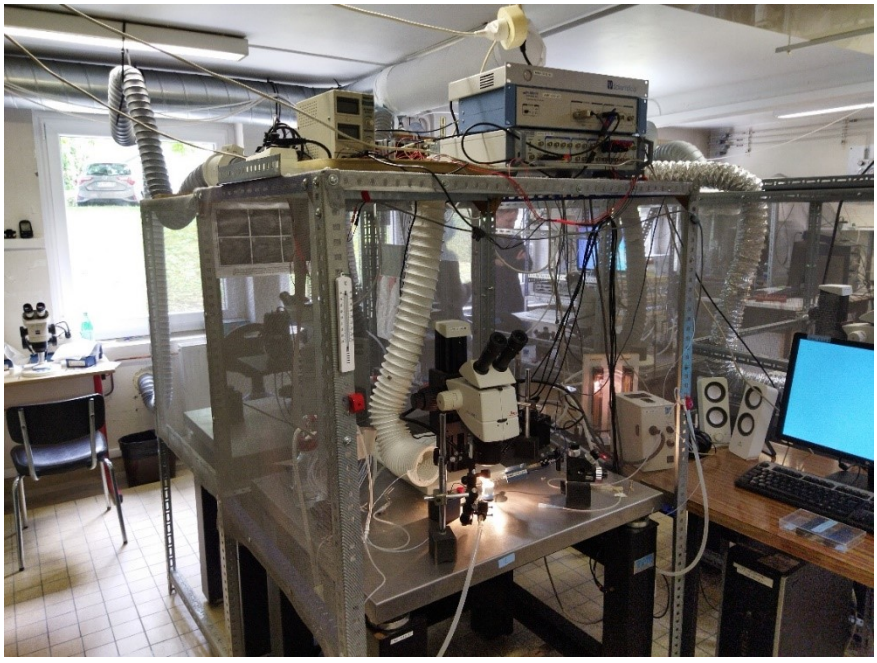

Figure 9: The experimental setup. Both clean and pheromone-infused air is delivered through separate tubes seen on the left side of the magnetic table. In the back, there is an air suction tube to avoid accumulation of the delivered pheromone. The insertion of microelectrodes is controlled with the use of a stereomicroscope seen in the middle and with the micromanipulator on the front right of the table. (Own photography, taken with the permission of Dr. P. Lucas.)

4.2. Data analysis

4.2.1. Formal description of the spike train

The first thing that has to be done when characterizing the neural response is to represent it in the form of a spike train. A spike train of n spikes can be represented mathematically by the neural response function $\rho(t)$,

$$\rho(t) = \sum_{i=1}^{n} \delta(t - t_i).$$

(1)

The times of individual spikes are denoted by t_i (where $i = 1,2,\dots,n$) and $\delta(t - t_i)$ is the Dirac delta function which is defined as

$$\delta(x) = \begin{cases} \infty \text{ if } x = 0 \\ 0 \text{ otherwise.} \end{cases}$$

(2)

In words, the neural response function assigns infinity to all the time points when spikes occur and zero to the rest of the interval. This way it "marks" the time of the spike occurrence. Typically, when the function is plotted, each spike is represented by an upward pointing arrow perpendicular to the horizontal time axis thereby indicating its infinite length, or by a dimensionless vertical dash.

4.2.2. Frequency code

To analyze a spike train from the frequency coding viewpoint essentially means to estimate its firing rate. The firing rate is the frequency in which a neuron fires action potentials and it is measured in the units of Hertz (Hz). There are several ways of extracting the firing rate from a spike train. The simplest approach is to count all the spikes in the spike train and divide the number by the duration of the spike train. This is particularly useful if we are not interested in the potential heterogeneities in the distribution of spikes along the spike train either because we dismiss it as noise or

because the information it might provide is not of any use for us. The operation can be expressed mathematically as

$$r = \frac{n}{T},$$

(3)

where n is the number of spikes and T is the duration of the spike train. In our case however, we need to employ more advanced methods that are able to capture such heterogeneities as our spike trains reflect temporal fluctuations of the stimulus whose effect needs to be analyzed in detail.

The easiest way to increase temporal resolution is by making T smaller, therefore dividing the spike train into multiple smaller time windows, and computing r for each of them separately. We call this process binning and such time windows bins. It needs to be said that decreasing the value of T typically increases the need for multiple trials. With only one trial, it would ultimately lead to the situation in which only one spike at maximum could fit into a bin and the firing rate could therefore gain only two possible values – 0 or T^{-1}. If we have multiple trials the chance of this happening is much lower. Another reason to work with multiple trials is that firing rates over short intervals are, due to stochasticity, often subjected to inter-trial variations and a value obtained from one trial can differ significantly from the trial average.

When using the binning method, we report the neural response in a peristimulus time histogram (PSTH) seen in Fig. 10B. The PSTH is formally described by the following piece-wise constant function

$$r(t) = \frac{\int_{t_i}^{t_i+\Delta t} \rho(t)dt}{\Delta t} \text{ for } t_i \leq t < t_i + \Delta t,$$

(4)

where $\rho(t)$ is the previously defined neural response function, Δt is the length of the bin and t_i indicates the left boundary or origin of the i-th bin. It is one of the two methods of firing rate estimation that we used in our analysis.

The other approach to estimating firing rates is by employing linear filtering. Linear filtering is accomplished through an operation called convolution which is the process of computing the integral of the product of two integrable functions f and g (after one is reversed and shifted). The general equation for convolution is

$$(f * g)(t) \coloneqq \int_{-\infty}^{+\infty} f(t-\tau)g(\tau)d\tau,$$

(5)

which, for the purpose of this thesis is used in the form

$$r(t) = \int_{-\infty}^{+\infty} \rho(t-s)k(s)ds,$$

(6)

where $k(s)$ is the so-called *kernel function* and $\rho(t-s)$ is the neural response function. The kernel function can be any well-behaved function satisfying $\int k(s)ds = 1$. We specifically used the Gaussian function, also called *the Gaussian kernel* with variance equal to σ^2,

$$k(s) = \frac{1}{\sqrt{2\pi}\sigma} exp\left(-\frac{s^2}{2\sigma^2}\right).$$

(7)

For the purpose of this thesis, we define the width w of the Gaussian kernel as $w = 2\sigma$. Because for a single spike occurring at time $t = t_i$ it follows from the definition of the delta function that

$$\int_{-\infty}^{\infty} \delta(t-t_i-s)k(s)ds = k(t-t_i),$$

(8)

it holds that for any t along the spike train, each spike contributes to the firing rate at that point by the value of the Gaussian function centered at t_i. By substituting the definition of $\rho(t)$ into the equation for $r(t)$, we obtain

$$r(t) = \sum_{i=1}^{n} k(t-t_i).$$

(9)

As a result, a continuous time-intensity curve is obtained. Basically, it is the same as if we would replace each spike with a Gaussian curve and then sum their values at a given time point. Because the integral of the Gaussian function is one, it represents an equal substitute to the original spike whose integral is also one. Therefore, the integral of the whole curve $r(t)$ is equal to the number of spikes.

The Gaussian curve can be thought of as a probability density function (PDF) which introduces uncertainty into the spike's occurrence by blurring it in time in such a way, that the probability density is highest in the original position of the spike and from there gradually decreases in both directions. By changing the value of w, we can modify the time resolution, the amount of detail in the curve $r(t)$. So, although the advantage of this method is that it eliminates arbitrariness in the placement of bins, the width of the kernels stays arbitrary.

Furthermore, the function $r(t)$ can be viewed not only as a firing rate estimate but also as an approximate time-course of the post-synaptic membrane potential (Gerstner & Kistler, 2002). In this case, we can think about a single Gaussian kernel as the contribution of a single spike to the membrane conductance change of the post-synaptic neuron. One could argue that in this case a spike shouldn't be represented by the bell curve as it "blurs" it both to the future and the past which is wrong because a spike can't make a contribution to membrane potential before it is fired. If our objective is to substitute a spike with its contribution to the membrane potential the more correct way to do that would be with an exponential curve that peaks in the time of the spike and then gradually declines, just like the real conductance would. According to Nawrot, Aertsen, and Rotter (1999), however, when analyzing a sufficiently dense spike train, the type of kernel being applied has virtually no effect on the resulting time course of $r(t)$. On the basis of this finding, we decided to keep using the Gaussian kernel.

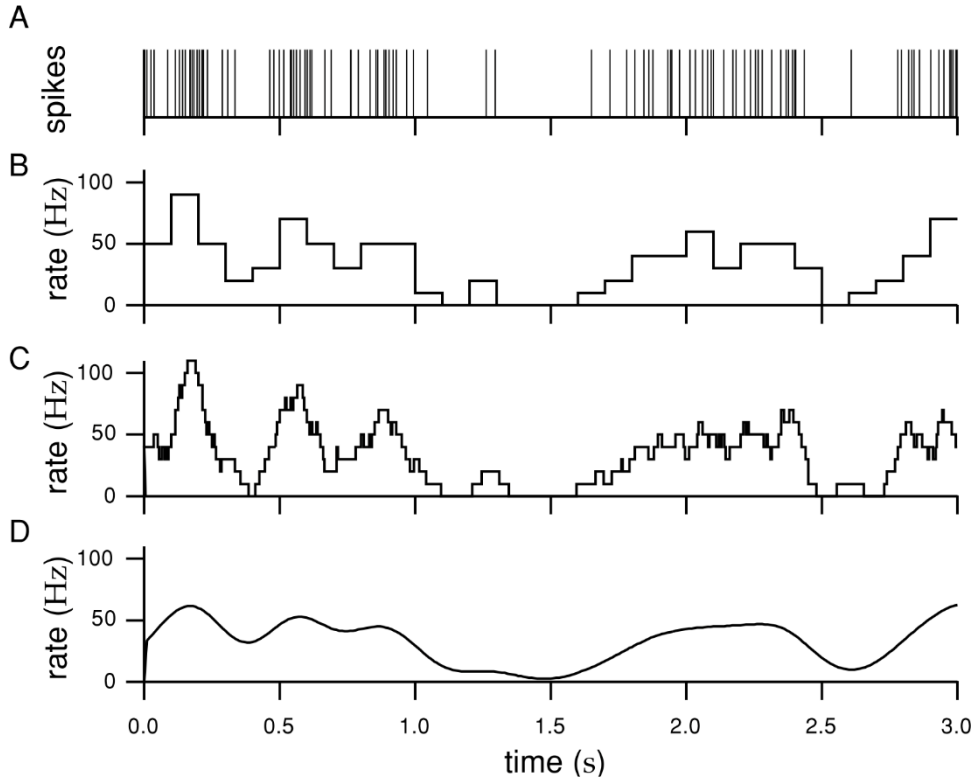

Figure 10: Different approaches to the neuronal firing rate estimation. (A) Experimental or simulated data: neuronal spike train, spikes are marked by vertical bars. (B) Firing rate estimate obtained by discretizing the time axis (binning) and counting spikes with a time window t = 100 ms. (C) Firing rate estimate determined by counting the spikes but this time by sliding the time window along the spike train. (D) Kernel-based firing rate estimation, computed by convolving a Gaussian function (zero mean and standard deviation of 100 ms) with the spike train response function. (Adapted from Dayan and Abbott (2001).).

4.2.3. Temporal code

While the description of neuronal activity from the rate coding point of view is relatively straightforward (Dayan & Abbott, 2001), the temporal code allows an infinite number of alternatives. Spike trains with equal firing rates may turn out to be different under various measures of the statistical structure of their interspike intervals (ISIs) (see, e.g., Kostal, Lansky, and Rospars (2007) and references therein).

For the purposes of this thesis, we mainly employ two complementary perspectives (Fig. 11) on the choice of ISIs that are used in the further analysis: 1) ISIs selected across trials at a given time, i.e., the instantaneous ISIs (Kostal, Lansky & Stiber, 2018), 2) consecutive ISIs in each trial (Shinomoto, Shima & Tanji, 2003).

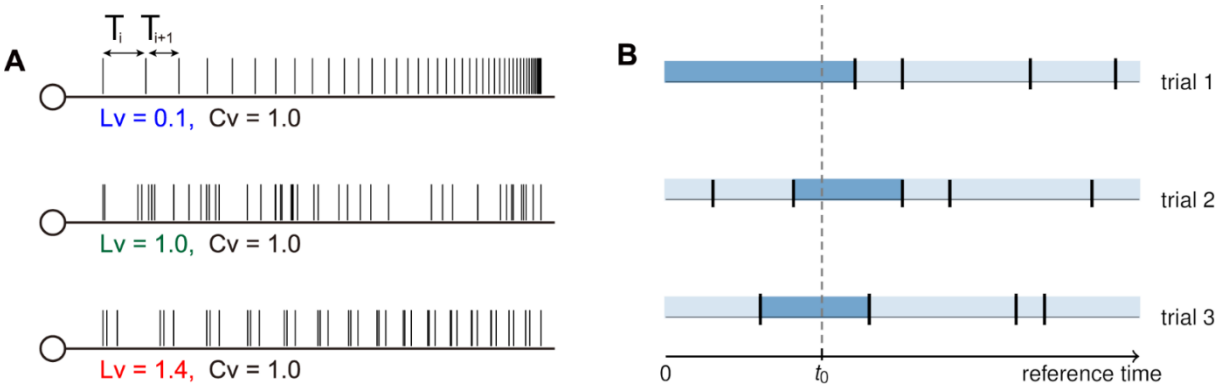

Figure 11: Different interspike intervals (ISIs) are selected for the purpose of the temporal code reliability and variability (A) Consequent ISIs in each trial (spike train) are employed to quantify the coefficient of local variability (Lv), to capture irregularities in ISI sequences (illustration shows identical sets of ISIs but with different ordering, slow or fast-changing). (B) To examine the temporal code reliability at a given time t_0, ISIs that contain t_0 are selected across multiple trials and further analyzed. (Adapted from Shinomoto et al. (2009) and Kostal, Lansky, and Stiber (2018).)

The analysis of instantaneous ISIs allows us to quantify the spike-timing reliability during stimulation at any given time. For that purpose, we employ different measures of statistical dispersion and their relative counterparts as explained in later sections.

On the other hand, the spiking patterns contained in the set of consecutive ISIs are not necessarily fixed to the reference (laboratory) time and therefore are speculated to provide an additional channel by which information may be transmitted by the temporal code between neurons (Shinomoto et al., 2009).

Local variation L_v of inter-spike intervals is a relatively recently invented/created statistic which characterizes spiking randomness. It has been proposed by Shinomoto, Shima, and Tanji (2003) as an alternative to the coefficient of variation C_v. Unlike C_v, it can discriminate distinct populations of cortical neurons based on their intrinsic rate-independent spiking properties. Both statistics result in 0 for regular spike trains with ISIs of constant length and 1 for spike trains where ISIs are independently exponentially distributed. While C_v detects the global variability of the whole ISI sequence, L_v detects the local stepwise variability of ISIs.

From the definition of L_v,

$$L_v = \frac{1}{n-1}\sum_{i=1}^{n-1}\frac{3(T_i - T_{i+1})^2}{(T_i + T_{i+1})^2},$$

(10)

where T_i is the length of the i-th interval, we can see that the summand is zero for two consecutive intervals of the same length and < 3 anytime else. The summand approaches zero with increasing length and decreasing difference in length. Contrarily, with increasing difference in length, the summand approaches 3. L_v is computed for individual trials. However, we are not primarily interested in the value of L_v itself, but in the variance of L_v between trials which can reveal a potentially common spiking architecture (Shinomoto et al., 2005) and is therefore suitable for the purpose of evaluating the spiking activity of ORNs in the context of the temporal coding hypothesis.

4.2.4. Measures of central tendency

This section as well as the following (4.2.5. Measures of variability) are concerned with further statistical analysis of data obtained by all the methods described above.

Mean: The arithmetic mean is the sum of a set of numbers divided by the count of numbers in the set. While the arithmetic mean is often used to report central tendencies, it is not a robust statistic, meaning that it is greatly influenced by outliers (values that are significantly larger or smaller than most of the values). Symbolically, if we have a data set consisting of the values $x_1, x_2, \ldots, x_n$, then the arithmetic mean μ is defined by the formula:

$$\mu = \frac{1}{n}\sum_{i=1}^{n} x_i$$

(11)

Median: The median is the value separating the higher half from the lower half of a data sample. It may be thought of as "the middle" value. The basic feature of the

median in describing data compared to the mean is that it is not skewed by a small proportion of extremely large or small values, and therefore provides a better representation of a "typical" value. The median can be defined as follows: For a data set x of n elements, ordered from smallest to greatest,

$$\mu_{1/2} = \begin{cases} x_{[(n+1)/2]}, & \text{if } n \text{ odd} \\ 1/2\left(x_{[n/2]} + x_{[(n+1)/2]}\right), & \text{if } n \text{ even.} \end{cases}$$

(12)

4.2.5. Measures of variability and relative dispersion

Most of the measures below tell us how much a set of values is dispersed around its average, or another measure of central tendency, in other words, whether they are concentrated around it or spread out to greater distances from it.

Standard deviation: Standard deviation (SD) is most commonly represented in mathematical texts and equations by the lower-case Greek letter sigma σ. The population standard deviation is the square root of the population variance. In cases where we cannot sample every member of a population, the population standard deviation is estimated by examining a random sample taken from the population and computing the sample standard deviation. The *uncorrected sample standard deviation* uses the standard formula for variance, that is the population variance formula, and it is a biased estimator. That is because using the population variance on a sample generally underestimates the population variance. Therefore, the population standard deviation is typically estimated using the *corrected sample standard deviation*

$$\sigma = \sqrt{\frac{1}{n-1}\sum_{i=1}^{n}(x_i - \mu)^2},$$

(13)

which is the square root of the *unbiased sample variance*. A useful property of the standard deviation is that, unlike the variance, it is expressed in the same units as the data. Furthermore, the distances from the mean are squared, so large deviations are weighted more heavily, and thus outliers can heavily influence it. From one perspective,

it can be considered to be a disadvantage. On the other hand, a more straightforward method of measuring data dispersion – the mean absolute deviation, which does not square the distances but only takes their absolute values and finds their mean, gives the same result not only for the mean but for any arbitrary value inside the sample range that we choose to measure the distances from. In statistics, however, we want our measure of dispersion to be smaller when calculated from the mean than from anywhere else. That is why standard deviation is preferred, even though it amplifies the effect of outliers on the overall deviation.

Coefficient of variation: While the variability may be measured simply by using the variance, or standard deviation respectively, the variance usually grows with the mean value. Instead, the relative measures of statistical dispersion are often employed, which relate the actual dispersion value to the mean (or another measure of central tendency) (Kostal, Lansky & Pokora, 2013). The most frequently used relative dispersion measure based on the standard deviation for positive random variables is the coefficient of variation

$$C_v = \frac{\sigma}{\mu}. \tag{14}$$

For example, the main advantage of C_v as the measure of ISI variability (as compared to variance) is that C_v is dimensionless and its value does not depend on the choice of units of ISIs (e.g., seconds or milliseconds) and therefore allows for a meaningful comparison of spike trains with unequal firing rates (Softky & Koch, 1993).

However, the value of C_v might not be a reliable indicator of dispersion for highly skewed data with mean close to zero – such situation can happen in our case when analyzing the firing rate, whose mean across trials can change between small and large values, especially during the fluctuating stimulation. Therefore, instead of taking the average value of C_v over the 2s stimulation, we evaluate the average standard deviation divided by the overall average firing rate, as explained in more detail in the Results section.

Interquartile range: The interquartile range, also referred to as the IQR, the midspread, or the middle 50%, is defined as the difference between the 75th and 25th percentiles of the data. To calculate the IQR, the data set is divided by three quartiles into four rank-ordered even parts. These quartiles are denoted as Q_1 (the lower quartile), Q_2 (the median), and Q_3 (the upper quartile). The lower quartile defines the 25th percentile and the upper quartile defines the 75th percentile, thus IQR = $Q_3 - Q_1$. The IQR can be clearly visualized by the box on the box-and-whisker plot. The advantage of this measure of dispersion is that it filters out outliers and it is, therefore, more robust that the standard deviation. For the purpose of the thesis, the quartiles were calculated by linear interpolation of the empirical cumulative distribution function (ECDF). The IQR divided by the median is denoted as rIQR and it is a robust alternative to the C_v (Arachchige, Prendergast & Staudte, 2022)

Median absolute deviation: The median absolute deviation (MAD) is defined as the median of the absolute deviations from the data's median. The MAD is a robust statistic, being more resilient to outliers in a data set than the standard deviation and even the IQR (Huber, 1981). It is defined as

$$MAD = median\left|x_i - \mu_{\frac{1}{2}}\right|. \quad (15)$$

Just like in case of IQR, we can define a MAD-based robust relative statistic rMAD which is the MAD divided by the median (Arachchige, Prendergast & Staudte, 2022).

Entropy: Entropy is a fundamental quantity of the information theory first postulated by Claude Shannon for discrete random variable (r.v.) X with a probability mass function $P(x_i) = \Pr(X = x_i)$, $i = 1,2,\dots n$. It represents the level of uncertainty inherent in the average outcome of a random variable. It can be thought of as the average number of maximally informative binary questions we need to ask to identify the outcome of X. The entropy $H(X)$ is a non-negative quantity defined as

$$H(X) = -\sum_{i=1}^{n} P(x_i)\log_2 P(x_i)$$

(16)

and the units of entropy are denoted as "bits". The larger the value of entropy, the more "unpredictable" or "random" are the outcomes of r.v. X. This formula is only applicable to discrete probability distributions such as those obtained by computing the spike-count firing rates.

Because entropy is a quantity that serves to describe populations, using a sample as the input does not give us correct results. In particular, it is well known that plugging the basic frequency estimate of $P(x_i)$ (i.e., the number of counts x_i occurs divided by the total number of observations) into Eq.(16) results in a negatively biased estimate (Basharin, 1959) Therefore, adjustments to the formula must be made to obtain an estimate of the actual population entropy. There are several estimators in existence that account for this issue. We specifically used the Chao-Shen estimator, which has been proposed in 2003 by ecologists Chao and Shen and whose original function was to estimate species diversity when the number of species and their abundance is unknown. The Chao-Shen entropy estimator is therefore suitable in our situation, as the maximal number of spikes in a time window is not known in advance. Let $\widehat{p_i}$ be again the basic empirical frequency estimate of the probability of the i-th value and f_1 the number of singletons (the number of times any value occurs only once in the sample). Then the Chao-Shen entropy estimator reads

$$\widehat{H}(X) = -\sum_{i=1}^{n} \frac{\pi_i \log_2 \pi_i}{1-(1-\pi_i)^n}$$

(17)

where $\pi_i = \left(1 - \frac{f_1}{n}\right) p_i$.

With continuous data such as those obtained by kernel firing rate estimation, a different approach however needs to be taken as the Eq.(16) (as well as the Chao-Shen estimator) only allows for discrete input values. The quantity analogous to (discrete) entropy, but

applicable to continuous probability distributions, is called the differential entropy. If a random variable X follows probability density function $f(x)$ then the differential entropy $h(x)$ is defined as

$$h(X) = -\int f(x) \ln f(x)\ dx,$$

(18)

where $\ln(\cdot)$ is a natural logarithm.

Despite the differential entropy being defined similarly to its discrete counterpart, the mathematical properties of $h(X)$ are very different. The value of $h(X)$ may be positive or negative, therefore it is not directly usable as a measure of random variable randomness or dispersion. Instead, the entropy-based dispersion measure σ_h is defined as (Kostal, Lansky & Pokora, 2013)

$$\sigma_h = \exp(h(X) - 1).$$

(19)

The interpretation of σ_h is described in detail in (Kostal & Marsalek, 2010), informally, the value is bigger for those random variables, which generate more diverse (or unpredictable) realizations. Furthermore, there is a connection between the value of standard deviation σ and σ_h: their values equal when r.v. X is distributed exponentially, in which case σ_h also attains its maximal possible value among all probability distributions with a given mean value. The corresponding relative dispersion is defined analogously to C_v

$$C_h = \frac{\sigma_h}{\mu}.$$

(20)

The estimation of C_h therefore requires the estimate of $h(X)$. It is generally preferable to avoid estimations based on data binning (histograms), as the introduced discretization significantly affects the results. In this thesis, we use the standard Vasicek estimator (Vasicek, 1976), which yields reliable results for a wide range of data (Esteban

et al., 2001; Miller & Fisher, 2003; Kostal & Pokora, 2012). We sort the observed samples x_i according to their value, and the Vasicek estimator is defined as

$$\hat{h} = \frac{1}{n}\sum_{i=1}^{n} \ln\left(x_{[i+m]} - x_{[x-m]} + ln\frac{n}{2m} + \varphi_{bias,}\right.$$

(21)

where $x_{[i+m]} = x_{[m]}$ for $i + m > n$ and $x_{[i-m]} = x_{[1]}$ for $i - m < 1$. The integer parameter $m < \frac{n}{2}$ is set prior to the calculation, roughly one may set m to be the integer part of $\sqrt{n}$. The bias correcting factor is

$$\varphi_{bias} = ln\frac{2m}{n} + \left(1 - \frac{2m}{n}\right)\Psi(2m) + \Psi(n+1) - \frac{2}{n}\sum_{i=1}^{m}\Psi(i+m-1),$$

(13)

where $\Psi(z)$ denotes the digamma function.

5. Results and discussion

5.1. Preliminary data analysis

First, we inspected the 78 data files for stability in time, abrupt changes, sudden termination, or any potential technical faults during the recording. We require that the spiking responses for the fluctuating and constant stimulation are comparable in the total number of spikes. Note that during the actual data analysis we use the relative dispersion measures which allow us to compare spike trains with different firing rates meaningfully.

All 78 recordings are shown together in Fig. 15, where the spike ordinal (serial) number is plotted against the time. It is obvious that some recordings end abruptly or exhibit instability in time. In the second case, the curve deviates from the dashed blue line whose slope is equal to the total spike count divided by the total recorded time (inter-trial breaks excluded) and which represents the idealized time progression when spikes are evenly spaced. Both types of "faulty" neurons were excluded immediately (e.g., cells: 19321000, 19218007, 19221000). The remaining cells were investigated in more detail, especially with regard to the average spike count and its similarity between the two stimulation types. Cells that showed a great level of dissimilarity were also excluded. Ultimately, 24 neurons were selected for the data analysis.

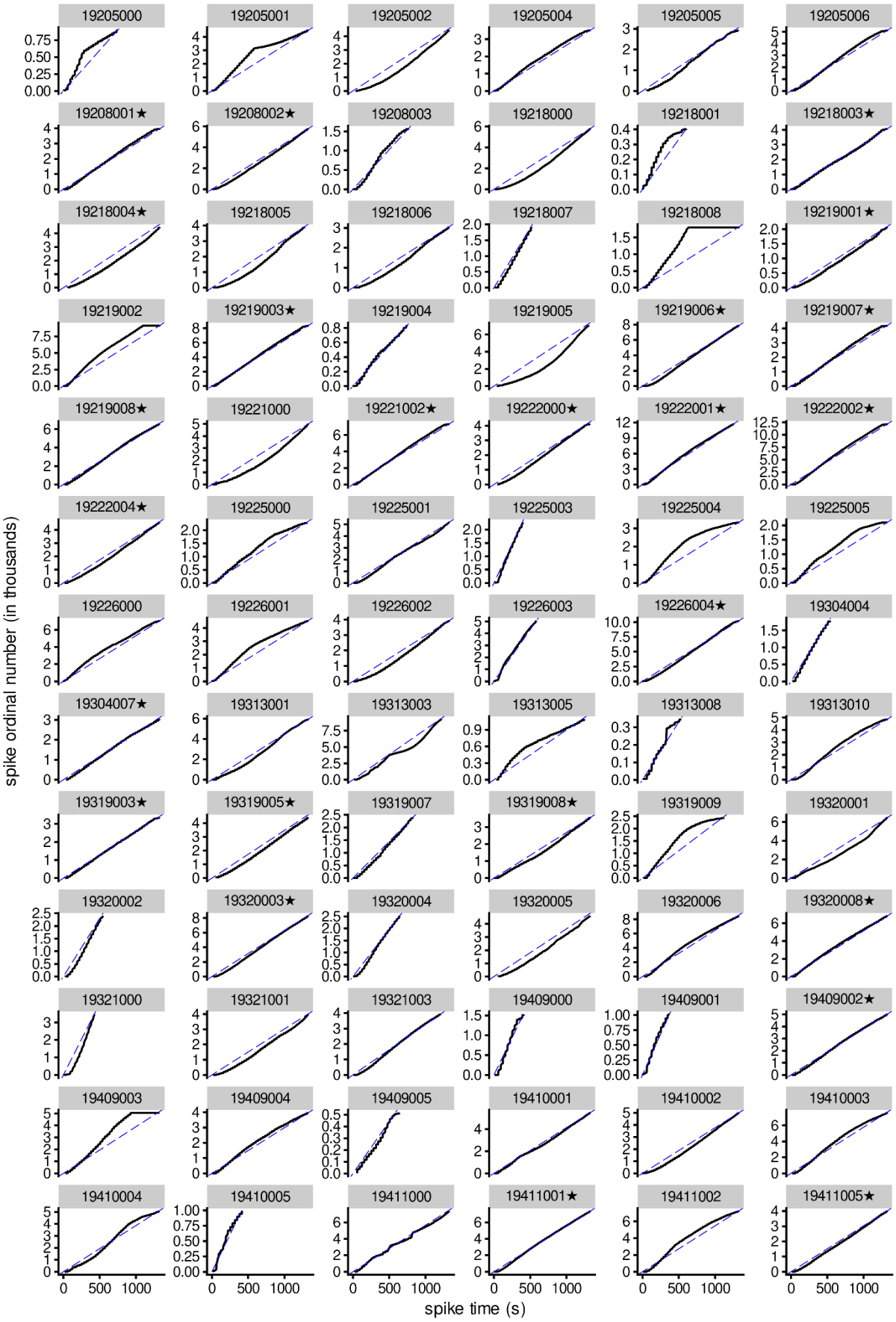

Figure 12: (caption on the next page)

Figure 12: (previous page) The dependence of spike ordinal number on the recording duration for all 78 neurons. See section 4.1. for more details on the experimental procedure. Several recordings end abruptly (e.g., 19321000, 19218007), and some show instability in time (e.g., 19221000, 19205000) as the spikes arrive with apparent deviation from the average given by the inverse of the mean ISI (dashed blue line). The 24 neurons finally selected for the analysis are marked by a star.

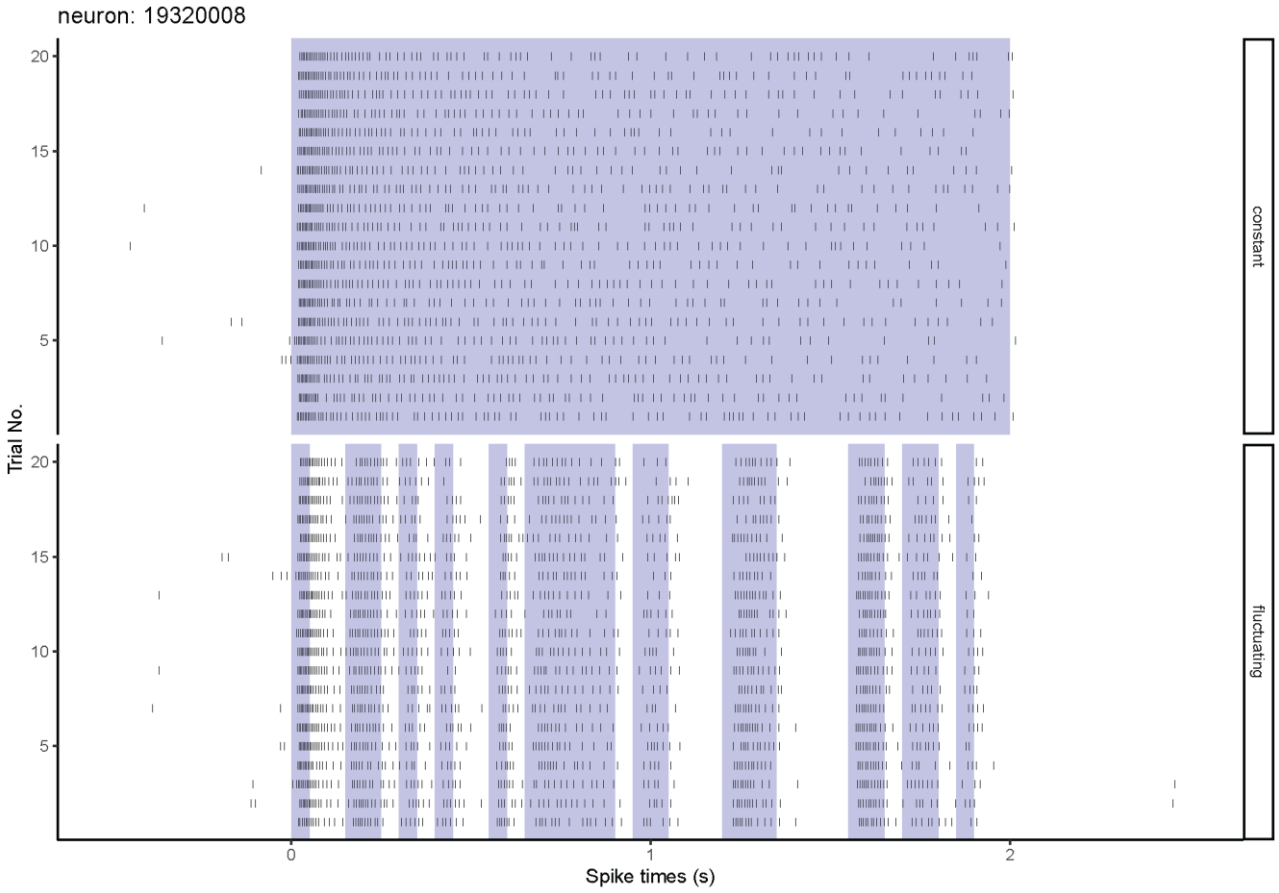

Figure 13: A typical ORN spiking response obtained from the experiment (spikes marked by vertical bars). Trials of constant and fluctuating 2s long stimulation alternated and were separated by 30s pauses, yielding 20 trials in total for each stimulus type. The shaded area marks the presence of the pheromone pulse (whiff). The average number of spikes obtained during either the constant or the fluctuating stimulation is approximately equal.

The average firing rates of the selected neurons for the *constant* and *fluctuating* stimulus types are shown in Fig. 14. The overall spread of the average firing rates across the population, which is most likely caused by the heterogeneity of the ORNs (Rospars et al., 2014), is relatively large despite using the same pheromone dose. Also, note that the firing rate in the fluctuating type is higher in most cases (22 out of 24).

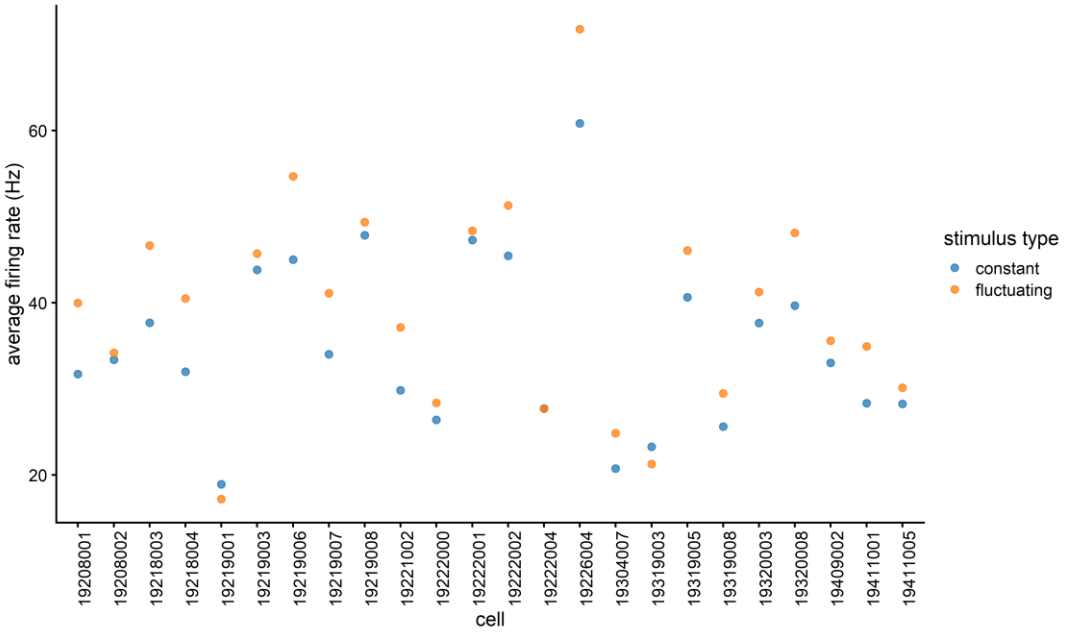

Figure 14: The average firing rates of the selected 24 ORNs. The relatively large spread of the firings rates across the ORN population, despite using the same dose in the experiment, is most likely caused by the reported ORN heterogeneity (Rospars et al., 2014).

5.2. Frequency code analysis

The firing rate response of ORNs to both stimulus types was first analyzed by using the binning (Eq. 4) and the kernel estimation (Eq. 9) methods. As the binning method introduces 'sharp' transitions into the estimation and compared to the more advanced kernel method it did not yield qualitatively different results, we present only the kernel-based method in the following text.

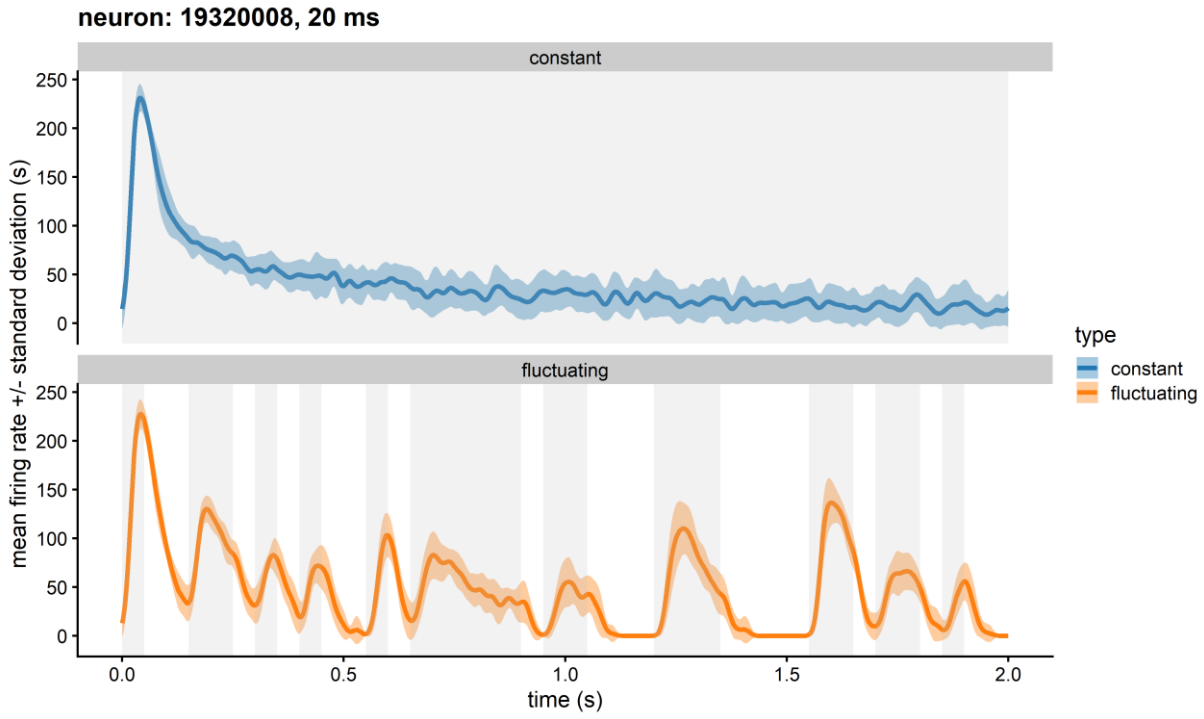

Figure 15: Typical ORN firing rate estimate using the 20ms Gaussian kernel for the constant and fluctuating stimulation types. The average firing rate (solid) and the standard deviation (shaded area) are calculated from 20 trials. (The same neuron is shown in Figs. 13 and 28).

As for the kernel-based method, we calculated the firing rate response reliability by performing the following procedures. First, for each ORN, we extracted the individual trials from the recording and sorted them according to their type (see Fig. 13). Second, for each of these trials, we estimated the firing rate using the Gaussian kernel (see section 4.2.2) of 4 different bandwidths, $w = \{10,20,50,100\}$ ms. The particular set of kernel bandwidths was chosen in order to investigate the ORN response reliability on substantially different timescales while maintaining biological relevance (Kobayashi, Tsubo & Shinomoto, 2009; Barta et al., 2022; Jarriault et al., 2010). This way, we obtained 20 firing rate estimates for each cell, stimulation type, and bandwidth. At any time t of the 2s stimulation interval, we were thus able to compute the current dispersion of the 20 estimates. From these data, we were finally able to determine the overall response reliabilities.

There are two approaches to the task. One may either average the relative dispersion measure (e.g., $C_v(t)$ of the firing rate estimates evaluated at time t) over the 2s

stimulation as $\langle C_v \rangle = \left\langle \frac{\sigma}{\mu} \right\rangle$, or average the standard deviation and the mean firing rate independently and then take the ratio as $\frac{\langle \sigma \rangle}{\langle \mu \rangle}$. In most cases, the mean or the median firing rate during the blanks within the "fluctuating response" was zero or close to zero, deeming the relative dispersion overestimated and unreliable. That is why we decided to also adopt the second approach and why it in fact proved to be preferable. However, for completeness, we provide the discussion and results for $\langle C_v \rangle = \left\langle \frac{\sigma}{\mu} \right\rangle$ and $\langle C_h \rangle = \left\langle \frac{c_h}{\mu} \right\rangle$ later in this section and in Fig. 24 and Fig 27.

First, we compared the response reliability to the two stimulation types of the whole ORN *population*. The results are summarized by employing the standard box-and-whisker plots (Fig. 16). We tested whether the two population responses are different by employing the unpaired Wilcoxon test. The p-values are shown in the upper-left corner of each plot. (First, we rejected the hypothesis that the 'fluctuating' and the 'constant' population responses follow the normal distribution by the Shapiro-Wilk test. Since the distribution of firing rates is expected to be highly skewed, the Shapiro-Wilk test was done only for confirmation.)

We observe that the ratio of the standard deviation to the mean and its spread gradually decrease with increasing kernel width. This is not surprising as with wider kernels the firing rate curve becomes more and more flat. Because at the same time, the two populations gradually more and more overlap, the p-value also increases. While the p-values of the first three kernel widths meet the condition for significance, the p-value of the 100 ms kernel falls slightly out of the significance range.

The partial overlap of the two groups in Fig. 16 might yield the impression that the difference between the two response types is not 'sharp' enough. However, the inspection of individual neurons reveals a remarkably clear trend (Fig. 17). The response reliability is higher for the *fluctuating* stimulus type for almost all neurons and time resolutions (kernel widths). The observation, while clear from the figure, is further confirmed by the paired Wilcoxon test with highly significant p-values. The only two

neurons (19219001 and 19319003) for which the reliability is slightly higher for the constant case, and moreover only for $w = 100$ ms (Fig. 17D) have:

a) lowest average firing rate (see Fig. 14),

b) higher average firing rate for the constant rather than fluctuating stimulus type.

On the other hand, the low firing rate itself cannot be the only reason, see e.g., the cell 19304007. The overlap on the whole population scale is most likely caused by the ORN heterogeneity, which leads not only to differences in average firing rates but also to differences in response variability and other properties among individual receptor neurons (Rospars et al., 2014).

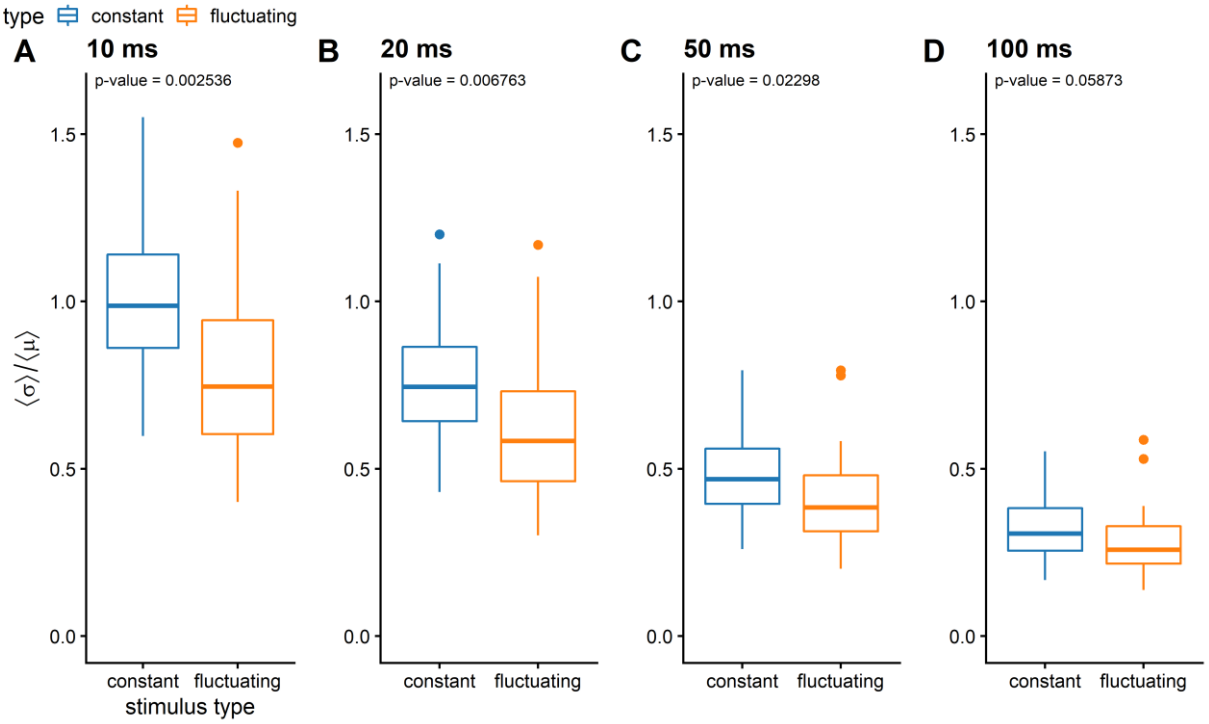

Figure 16: Relative standard deviation of the ORN firing rate, responding either to the fluctuating or constant stimulus. The ratio of the standard deviation to the mean and its spread gradually decrease with increasing Gaussian kernel width (10, 20, 50, and 100 ms), as the firing rate curves become more and more flat. The partial overlap in the response of the whole population to the two stimulus types is caused by the ORN heterogeneity. The unpaired Wilcoxon test was used to examine the hypothesis that the two response samples come from the same population.

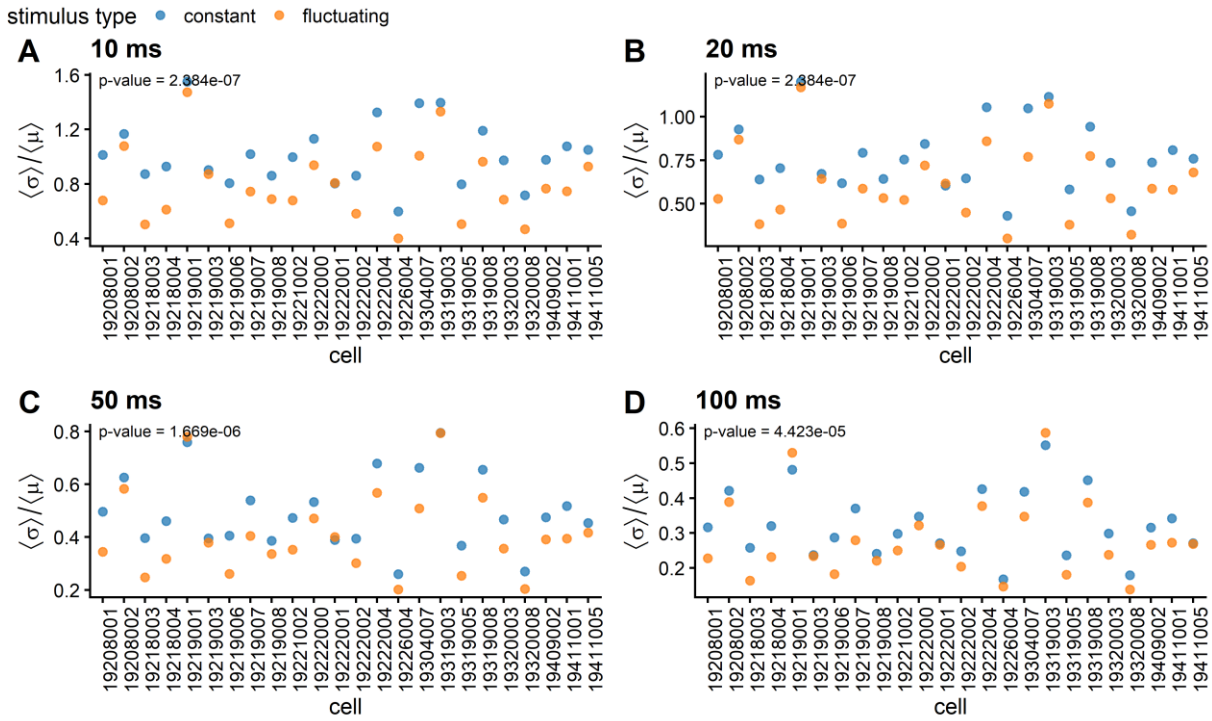

Figure 17: Detailed look at the relative standard deviation of the ORN firing rates of individual neurons. When compared to the whole population response (Fig. 16) it is clear that the response reliability to the fluctuating stimulus type is almost always higher for all selected neurons and time resolutions (kernel widths). The observation is further confirmed by the paired Wilcoxon test (p-values shown in the upper-left corner).

Qualitatively similar results were obtained also for another measure of relative dispersion, the relative interquartile range rIQR, i.e., the mean IQR to the mean median (averaged over the 2s stimulus duration), Figs. 18 and 19. The reason for choosing this particular statistic is motivated by the need to suppress the effect of outlying firing rate values since both the interquartile range and median are considered to be robust statistical descriptors (Huber 1981; Arachchige, Prendergast & Staudte, 2022).

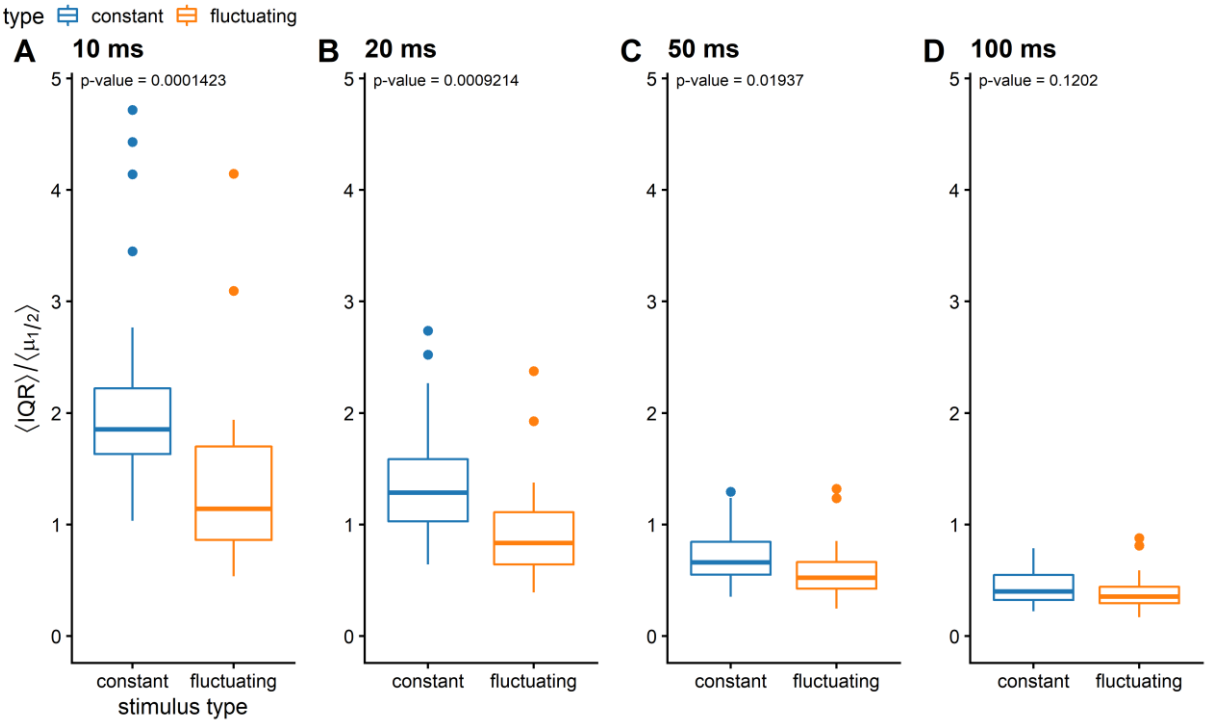

Figure 18: Relative dispersion of the ORN firing rate measured by the ratio of the inter-quartile range (IQR) to the median of the firing rate, averaged over the 2s stimulus duration. The results are qualitatively comparable with Fig. 16.

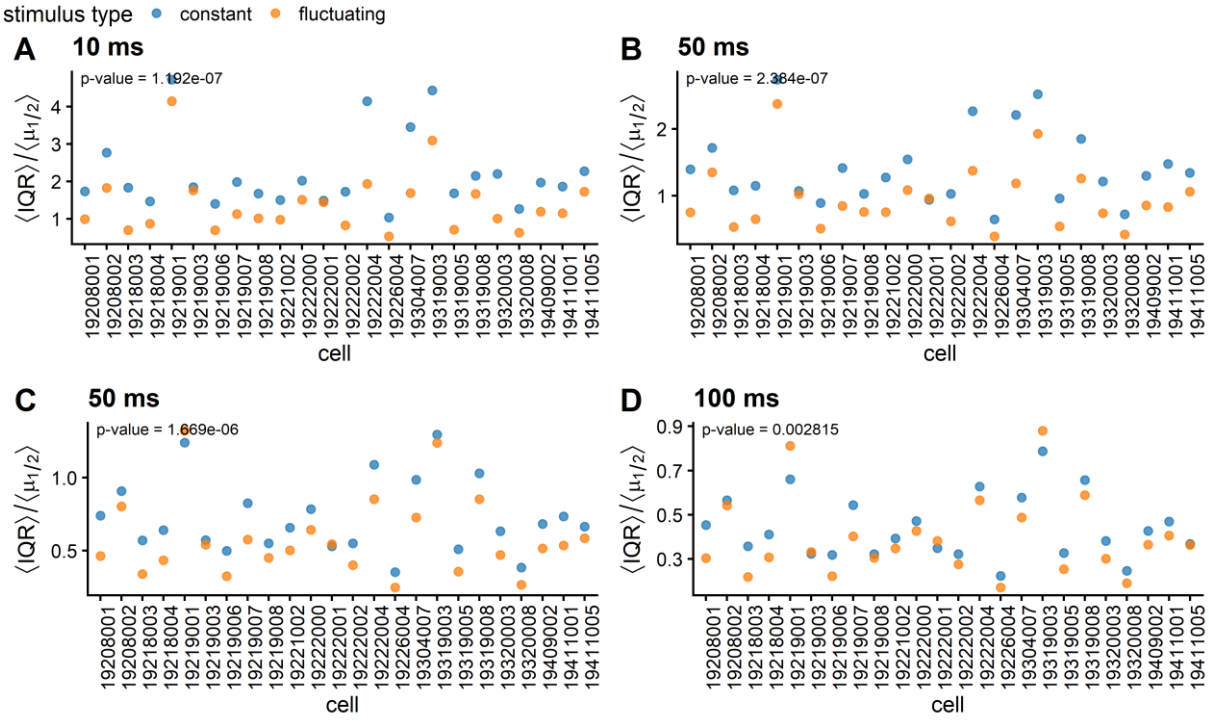

Figure 19: Relative dispersion of individual ORN firing rates measured by the ratio of the inter-quartile range (IQR) to the median of the firing rate (averaged over the 2s stimulus duration). The results are qualitatively similar to Fig. 17.

However, with the third statistic – mean MAD to mean median (Arachchige, Prendergast & Staudte, 2022), the situation changes as for the 10 ms kernel the two populations not only completely overlap, but a closer look at the individual neurons shows us that in more than half of the neurons the values of dispersion are even greater for the case of fluctuating stimulation (Figs. 20 and 21). It is because firing rate estimates computed with 10 ms kernels are too fine-grained for the MAD statistics. In situations when half of the data are zero or near-zero values, MAD is as well. The firing rate estimate with the 10 ms kernel is, especially in the low-frequency neurons, close to zero in more than 50% of trials. With kernels of bandwidths larger than 10 ms, the ratio of MAD to the median is qualitatively similar to the previous statistics.

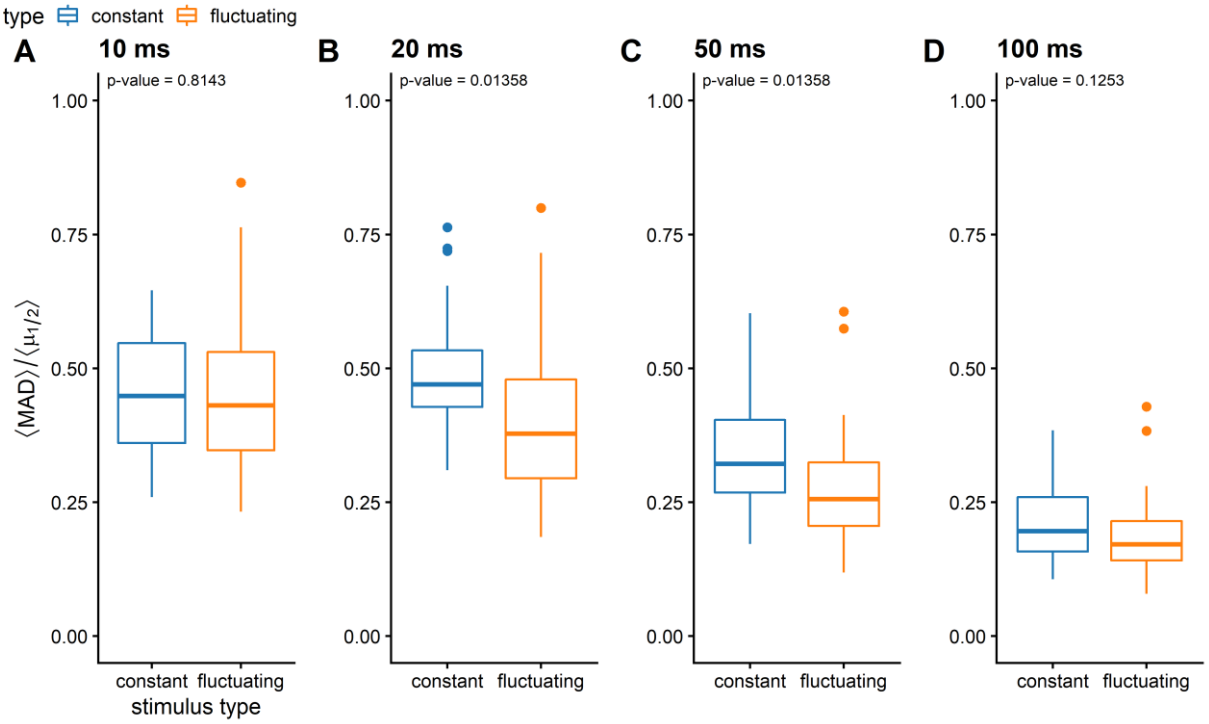

Figure 20: Response reliability of the ORN firing rate measured by the ratio of the median absolute deviation to the median of the firing rate, averaged over the 2s stimulus duration. The results are slightly different than in Figs. 16 and 18. For the 10 ms kernel, the two populations overlap, and in more than half of the neurons the values of $\langle \text{MAD} \rangle / \left\langle \mu_{\frac{1}{2}} \right\rangle$ are greater than for the case of fluctuating stimulation.

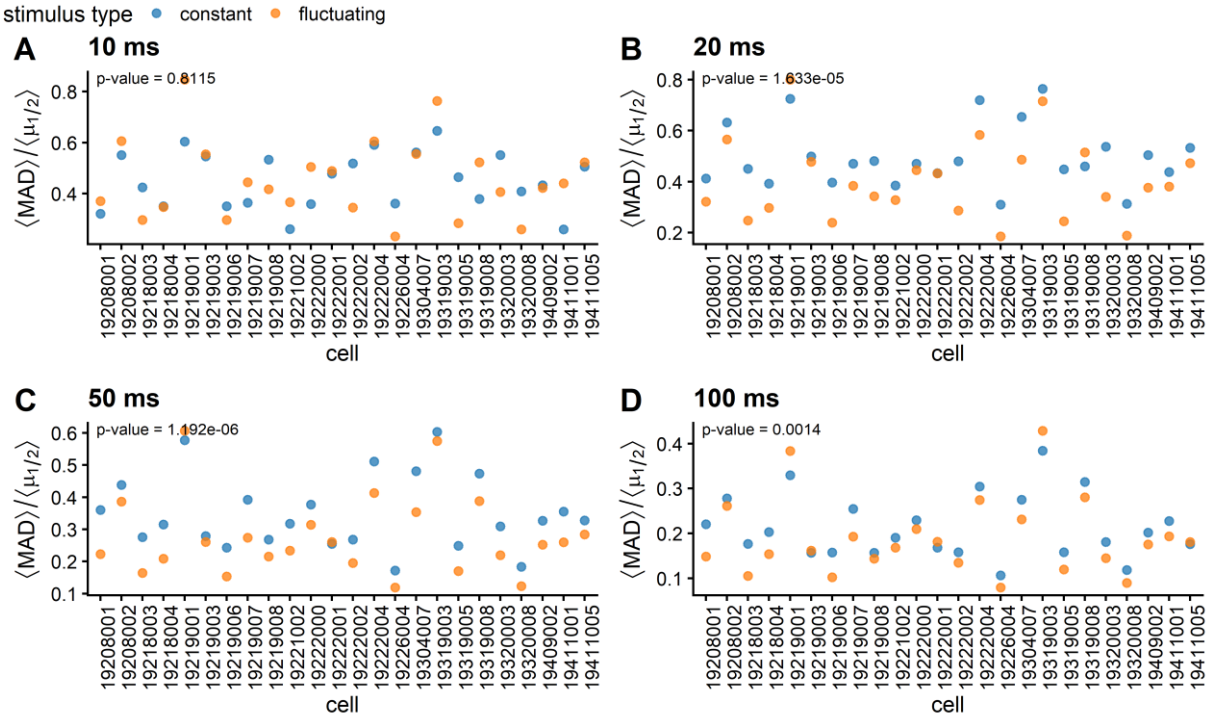

Figure 21: Individual ORN response reliability measured by the relative median absolute deviation. For the 10ms kernel width (A) the ORN responses do not show systematically greater reliability for the fluctuating stimulus type, due to the properties of the MAD dispersion measure (too sparse data due to the small kernel width).

The last measure of the response reliability is based on the concept of entropy, and thus rather independent from the previously considered measures, which are based either on statistical moments or quantiles (Kostal, Lansky & Pokora, 2013; Kostal, Lansky & Rospars, 2007). As the firing rates estimated by the kernel method are continuous, we employ the Vasicek estimator of differential entropy to estimate the dispersion σ_h as explained in section 4.2.5.

We see in Fig. 22A that the response dispersion of the population can be apparently higher for the fluctuating case. However, the results obtained with the 10 ms kernel are problematic for similar reasons as for the relative mean absolute deviation. In this case, the necessary continuity conditions for the Vasicek estimator do not hold (Beirlant et al., 1997) as frequent occurrence of zero, or values close to zero, leads to infinite differential entropy. Therefore, we consider the results obtained with a 10ms kernel to be unreliable for the entropy-based dispersion measure.

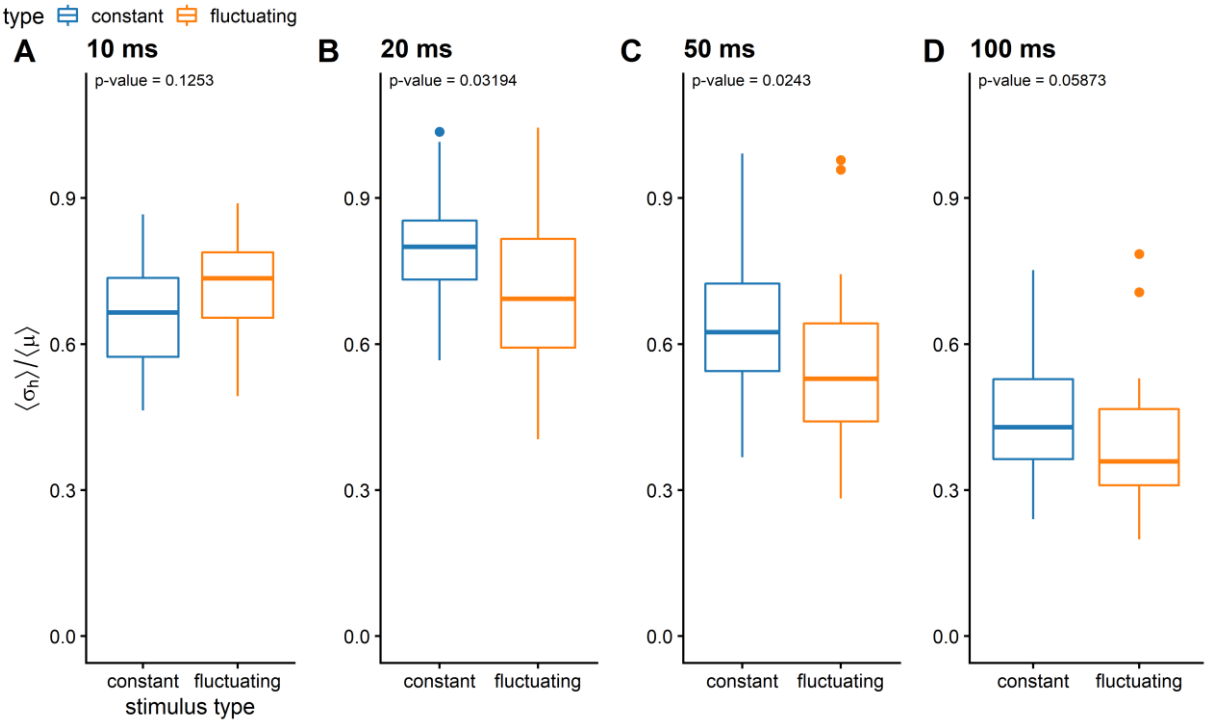

Figure 22: Response reliability of the ORN firing rate measured by the ratio of the entropy-based dispersion to the mean of the firing rate, averaged over the 2s stimulus duration. The results are comparable to Fig. 20. The 10 ms kernel results are not reliable due to the sparseness of the data.

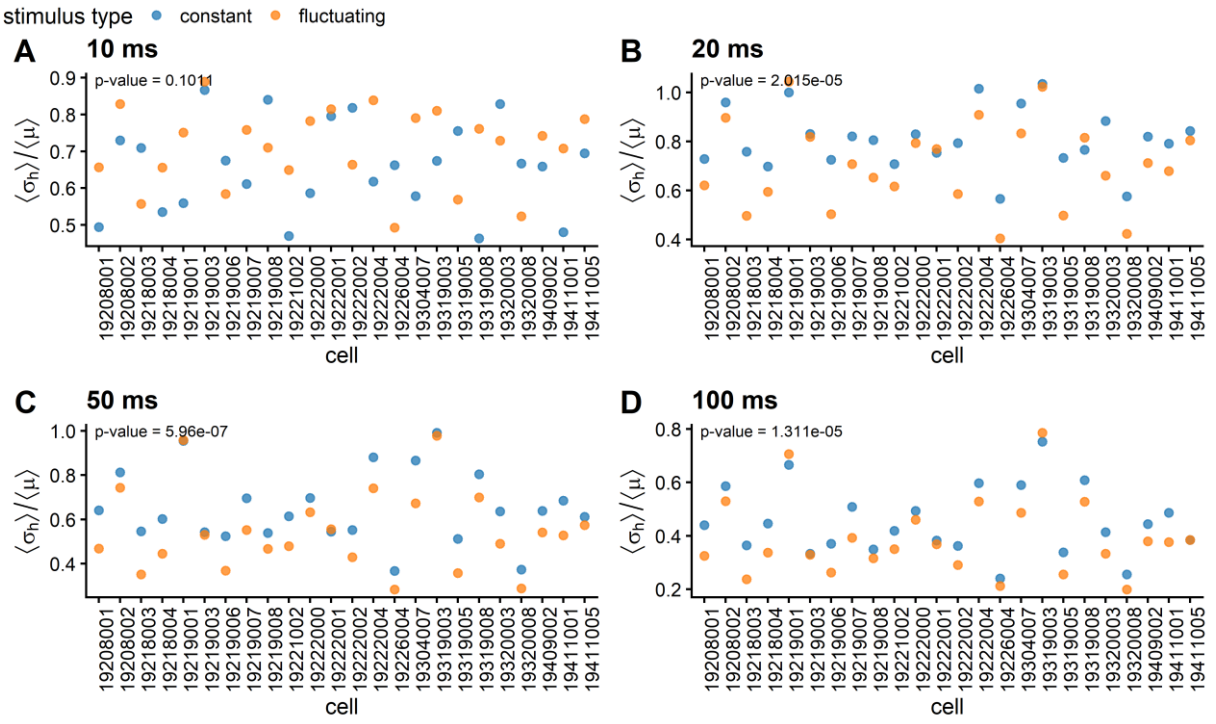

Figure 23: Individual ORN response reliability measured by the ratio of the entropy-based dispersion to the mean. For the 10ms kernel (A) the ORN responses do not show systematically greater reliability for the fluctuating stimulus type due to the properties of the entropy-based dispersion measure (too sparse data due to the small kernel width).

Note that for all statistics that were discussed above it holds true that the response variability of the two low-frequency neurons (19219001 and 19319003) stands out above the response variability of all the other neurons, both in the fluctuating and the constant stimulation case. On the other hand, the neuron with the highest average firing rate (19226004) systematically shows one of the lowest values of relative dispersion. These findings support the idea that during periods of high firing rate the presence of the refractory period limits the variability of the response, as the neuron steadily fires at peak frequency. This physiological mechanism could, therefore, represent a potential cause of the observed discrepancies in the response reproducibility between the two stimulation types. However, the refractory period by itself cannot be the all-encompassing cause, as it does not explain the response differences present in the low-frequency neurons.

Finally, for completeness, we present the results for the coefficient of variation and the entropy-based relative dispersion when evaluated at each stimulation time t and averaged over the entire 2s stimulus duration, i.e.,

$$C_v = \left\langle \frac{\sigma}{\mu} \right\rangle, \quad C_h = \left\langle \frac{\sigma_h}{\mu} \right\rangle.$$

The computation of the coefficient of variation provided us with results opposite to those obtained with the standard deviation (Fig. 24). The cause of this contrast lies in the presence of "quiet" episodes within the response to the fluctuating stimulation. In a hypothetical state in which $n-1$ out of n samples are zero and one sample is any non-zero value then $C_v = \sqrt{n}$. This is the highest possible value that the C_v of a sample can acquire. Also, such behavior of C_v does not intuitively comply with the expectations about 'variability' as with growing n the only non-zero sample becomes rarer and rarer. With 20 samples the C_v is therefore $\sqrt{20} \doteq 4.47$. Similar situations are common within fluctuating responses, where in most of the trials the rates are very close to zero, while only few values deviate due to the presence of an isolated spike. In the context of our data, the C_v therefore turned out to be an uninformative statistic as it puts great weight on variability that is in the absolute sense negligible.

On the other hand, the values of the entropy-based relative dispersion, C_h, are apparently more robust, not exhibiting the counter-intuitive behavior of C_v discussed above (Fig. 26). In summary, the conclusions obtained by examining $\frac{\langle \sigma_h \rangle}{\langle \mu \rangle}$ or $\left\langle \frac{\sigma_h}{\mu} \right\rangle$ are qualitatively similar.

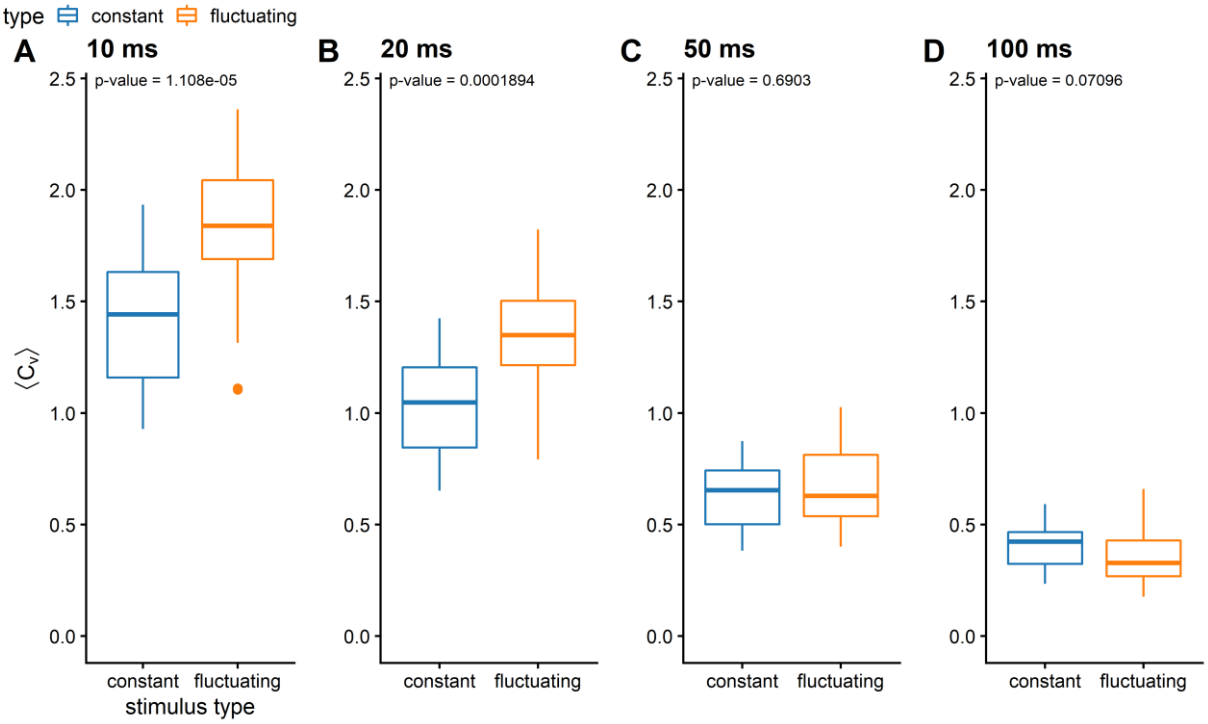

Figure 24: Response reliability of the ORN population firing rate quantified by the coefficient of variation, C_v, when evaluated at each stimulation time t and average over the entire 2s stimulus duration. Note the qualitative difference of the results when compared with Fig. 16, caused by the behavior of C_v for samples dominated by small values (as discussed in the text).

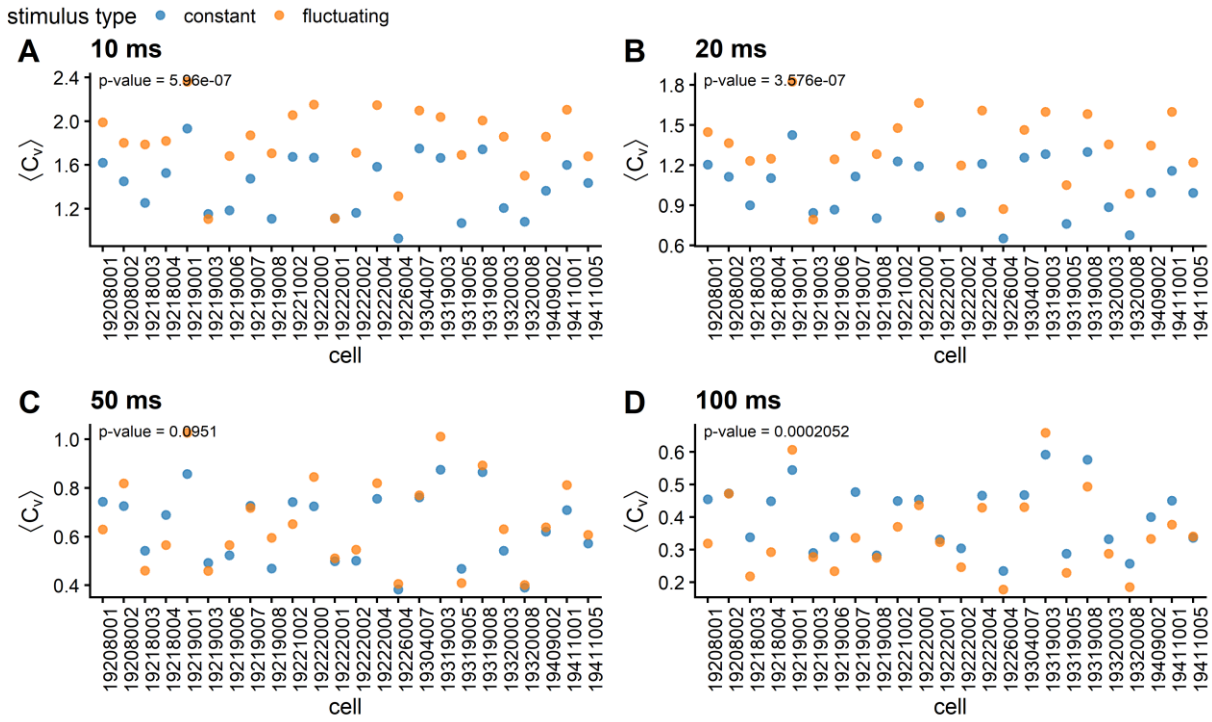

Figure 25: Response reliability of the individual ORNs, quantified by C_v (see also Fig. 24).

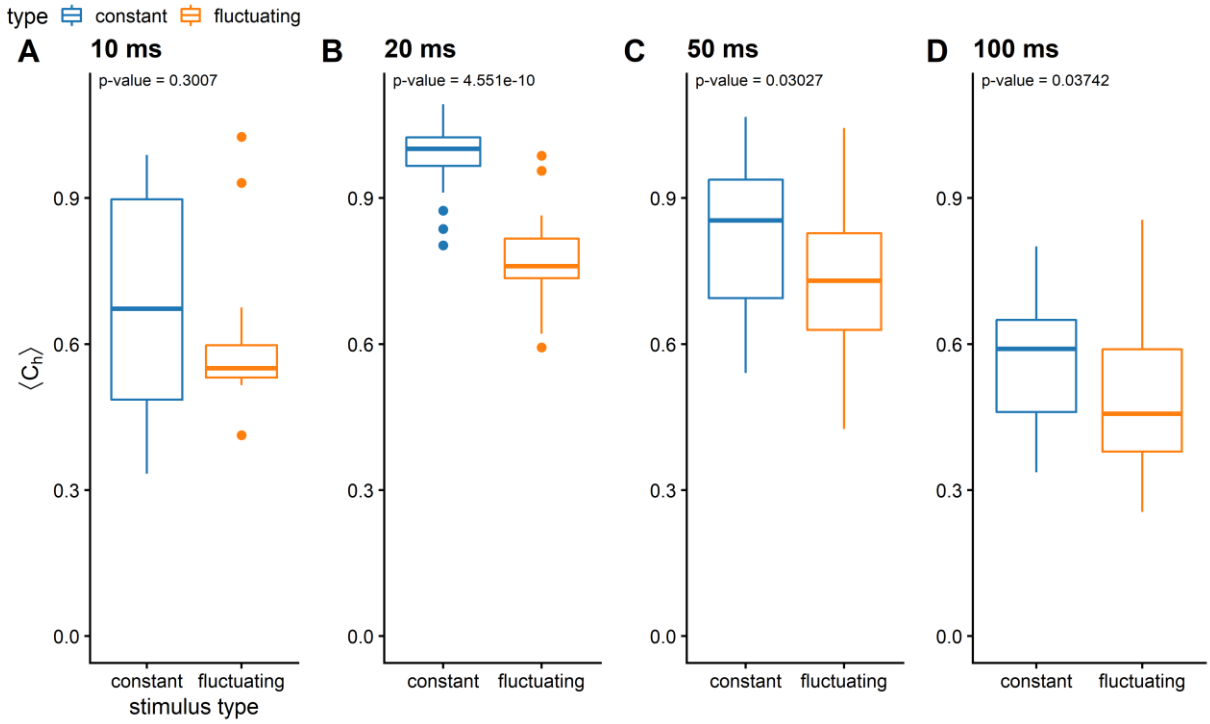

Figure 26: Response reliability of the ORN population firing rate quantified by the entropy-based relative dispersion coefficient C_h, evaluated at each stimulation time t and average over the entire 2s stimulus duration.

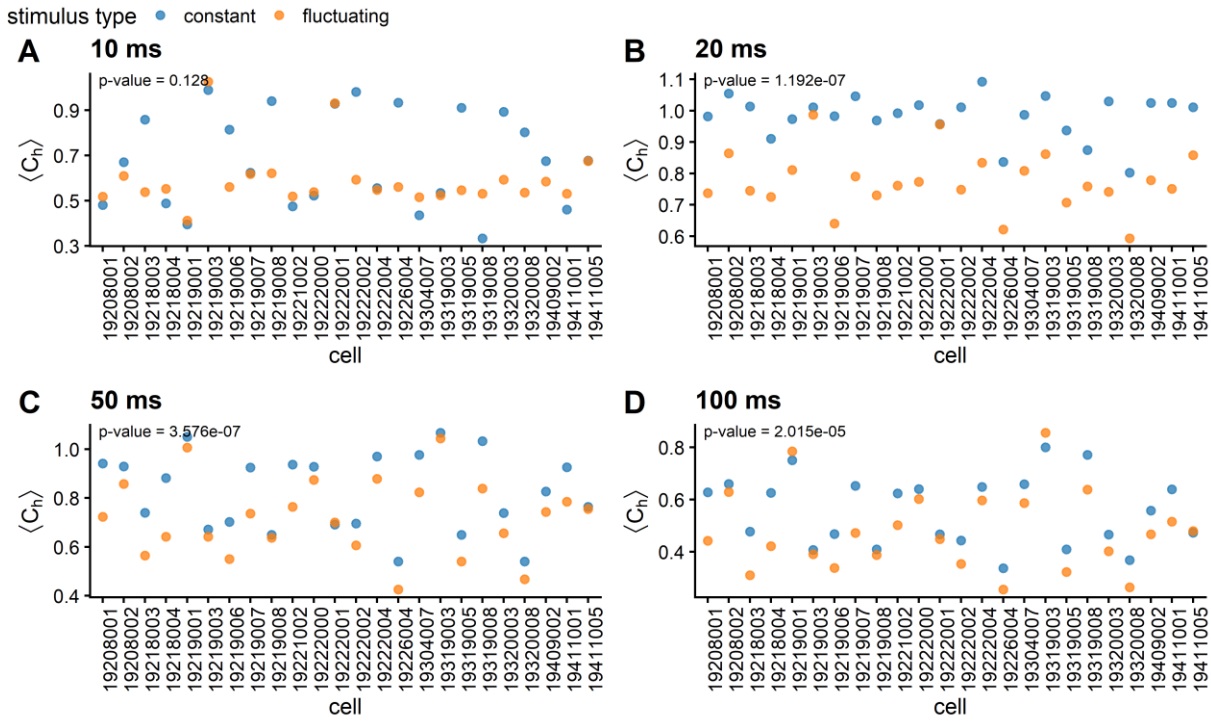

Figure 27: Response reliability of the individual ORNs, quantified by C_h (see also Fig. 26).

5.3. Temporal code analysis

The temporal code response of ORNs to both stimulus types was analyzed by using the two complementary perspectives described in section 4.2.3, see also Fig. 14.

First, we selected the ISIs across trials at a given time (the 'instantaneous' ISIs, see Fig. 28) and calculated the relative dispersion measures in order to quantify the reliability of the response from the temporal perspective. Note that there are several important differences with respect to the frequency code analysis presented above:

1) there is no bin or kernel width involved, the timescale of the temporal code is set automatically by the ISI duration,

2) the relative dispersion measures do not need to be adjusted because both the mean and the median ISI are (by definition) never zero and always greater than the absolute refractory period.

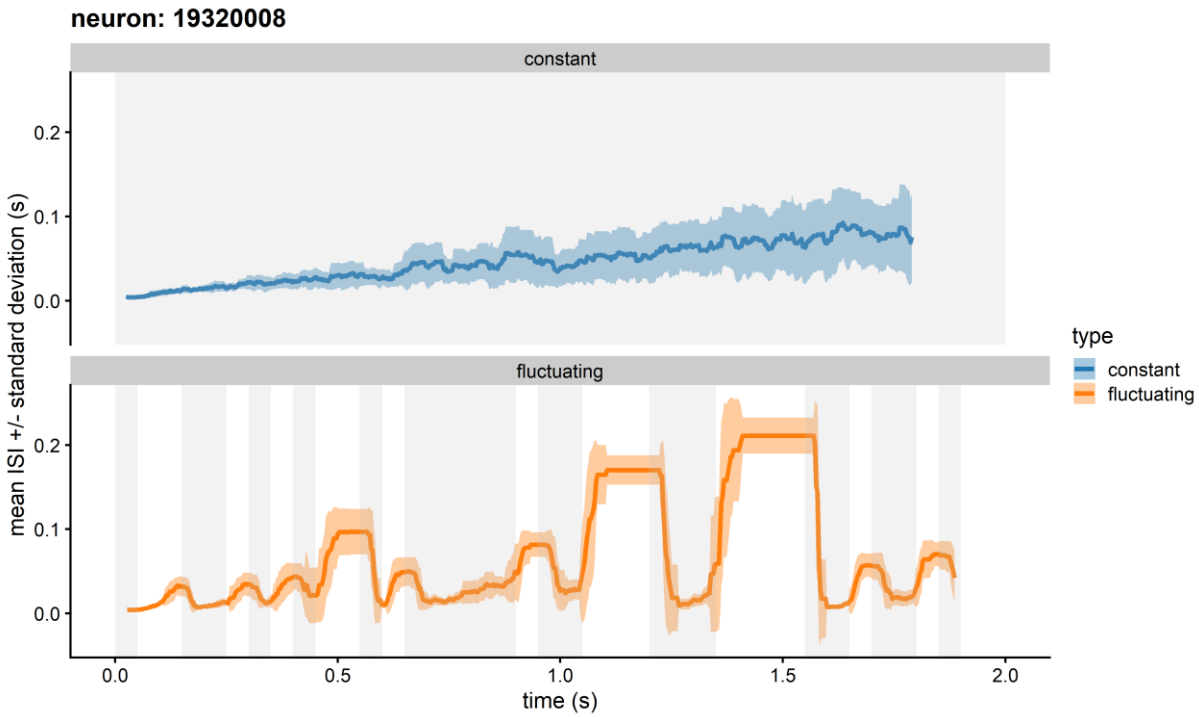

Figure 28: Typical response of ORN to the constant and fluctuating stimulation types. The average instantaneous interspike interval (solid line) and the standard deviation (shaded area) are plotted for the 2s stimulus duration. Note that the average ISI tends to increase due to neuronal adaptation. (The same neuron is shown in Figs. 12 and 15).

We present the results for both types of relative measures (the average of the ratio or the ratio of the respective averages) in order to provide results comparable to those obtained with the frequency code approach. Also, the unpaired and paired Wilcoxon tests were used for the population and individual ORNs analysis respectively.

The first type of relative dispersion measures, $\langle C_v \rangle$, ⟨rIQR⟩ ⟨rMAD⟩ and $\langle C_h \rangle$, are summarized in Fig. 29 for the whole population, and in Fig. 30 a more detailed look at individual cells is presented. The comparison of Figs. 29A and 29D highlights the difference between the *variability* and *randomness* as two different measures of dispersion. The population responses to the fluctuating and constant stimulus types are overlapping entirely when measured by C_v (p-value ca. 0.13) while a prominent difference is revealed on the C_h scale (p-value ca. 6×10^{-8}). This difference can be attributed to the intrinsic properties of the two measures (Kostal, Lansky & Rospars, 2007; Kostal, Lansky & Pokora, 2013), i.e., the same variability can be achieved with very different 'predictability' of the responses, especially for distributions generating outlying observations. Note that the measures $\langle C_v \rangle$ and $\langle C_h \rangle$ are averaged over the 2s stimulus course. At any time point, the constant stimulus type tends to generate more uniformly distributed ISI values while the fluctuating type generates more extremal ISIs (very short and long). Thus, while the average ISI may be comparable, C_h and C_v are highly different. Therefore, on the scale of $\langle C_h \rangle$ the two population responses are remarkably different. It is interesting to note, however, that even though the population response measured by $\langle C_v \rangle$ overlaps for the two types of stimulus, there is a significant trend on the level of individual neurons (Fig. 30A), i.e., the average C_v is almost always higher (p-value ca. 0.02) for every neuron for the constant stimulus type. Similar overlap as for C_v exists on the rIQR scale, not only for the population (p-value ca. 0.7) but also there is no significant trend on the level of individual neurons (p-value ca. 0.7).

We presume that the striking contrast between rIQR and rMAD is due to the different intrinsic properties of the two statistics, particularly due to their different sensitivity to outliers. Therefore, the high response variability typical for the whiff-blank

transitions causes the response to the fluctuating stimulus to be on average more variable when analyzed by rIQR than when rMAD is calculated.

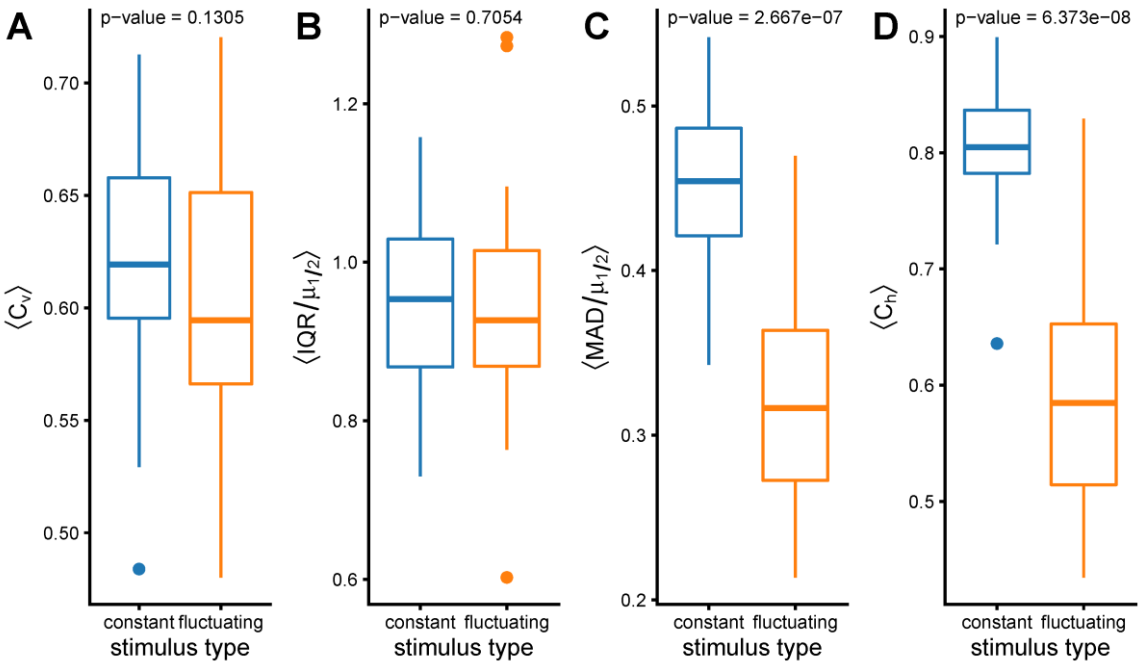

Figure 29: Response reliability of the ORN population based on instantaneous ISIs and quantified by computing the averages of relative dispersion measures. Note the striking contrast between $\langle C_v \rangle$ and $\langle C_h \rangle$.

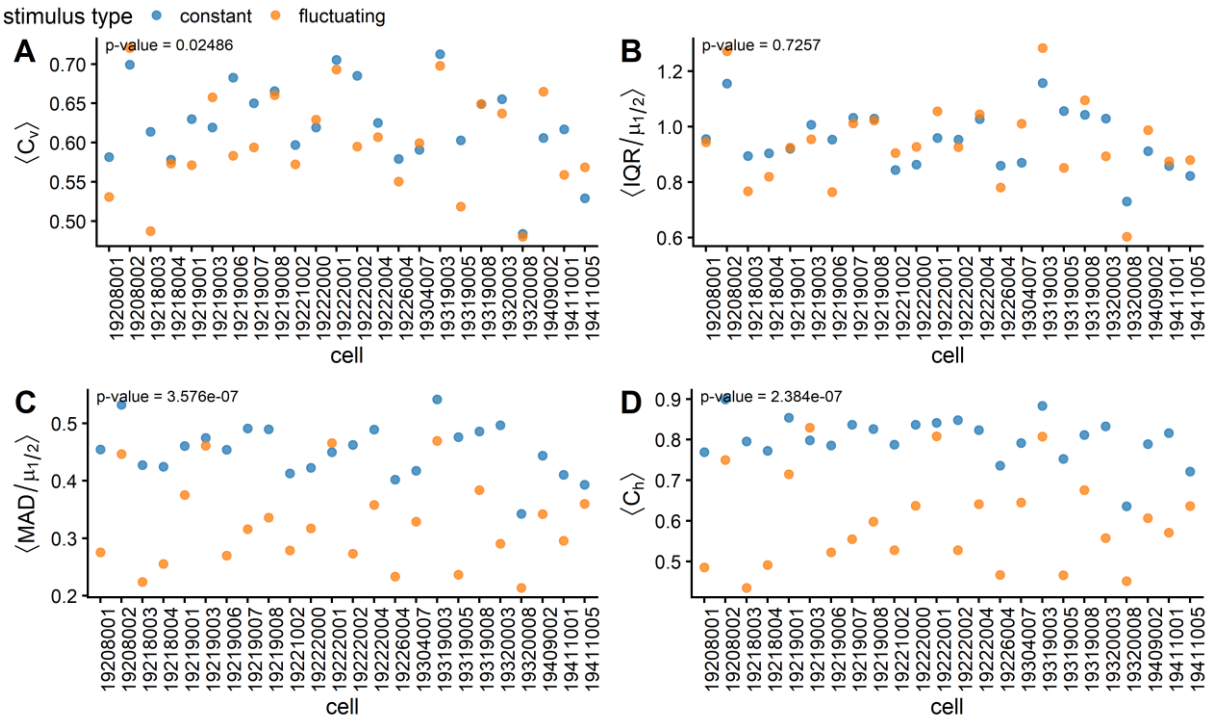

Figure 30: Response reliability of the individual ORN based on instantaneous ISIs and quantified by several dispersion measures.

The recently described post-stimulation inhibition period in ORNs (Barta et al., 2022) dramatically lowers the variability during the blank phase of fluctuating stimulation by increasing the ISI length. For example, see Fig. 28 where the average ISI length in the fourth blank (occurring at ca. 0.5s) is much larger than during the first blank of similar duration. Especially for neurons with a low average firing rate, this effect contributes significantly to increasing the response reliability for the natural-like, intermittent pheromone stimulation.

We also present results for the second type of the relative dispersion measure (the ratio of the respective averages) in Figs. 31 and 32. The difference between the constant and fluctuating stimulus types is clearly distinguishable both on the level of the ORN population and, consequently, on the level of individual neurons. The main reason lies in the fact, that the effect of high variability due to the mixture of short and long ISIs (as described above) is suppressed.

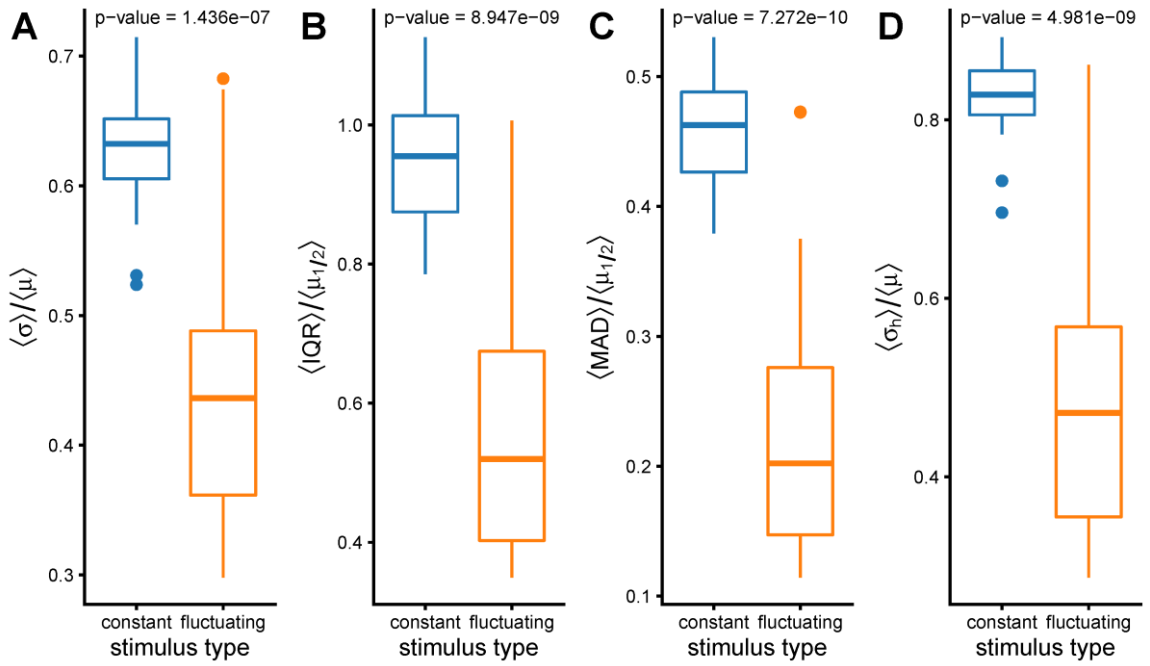

Figure 31: The population results for the second type of dispersion measures, i.e., the ratio of the mean dispersion to the mean/median of instantaneous ISIs.

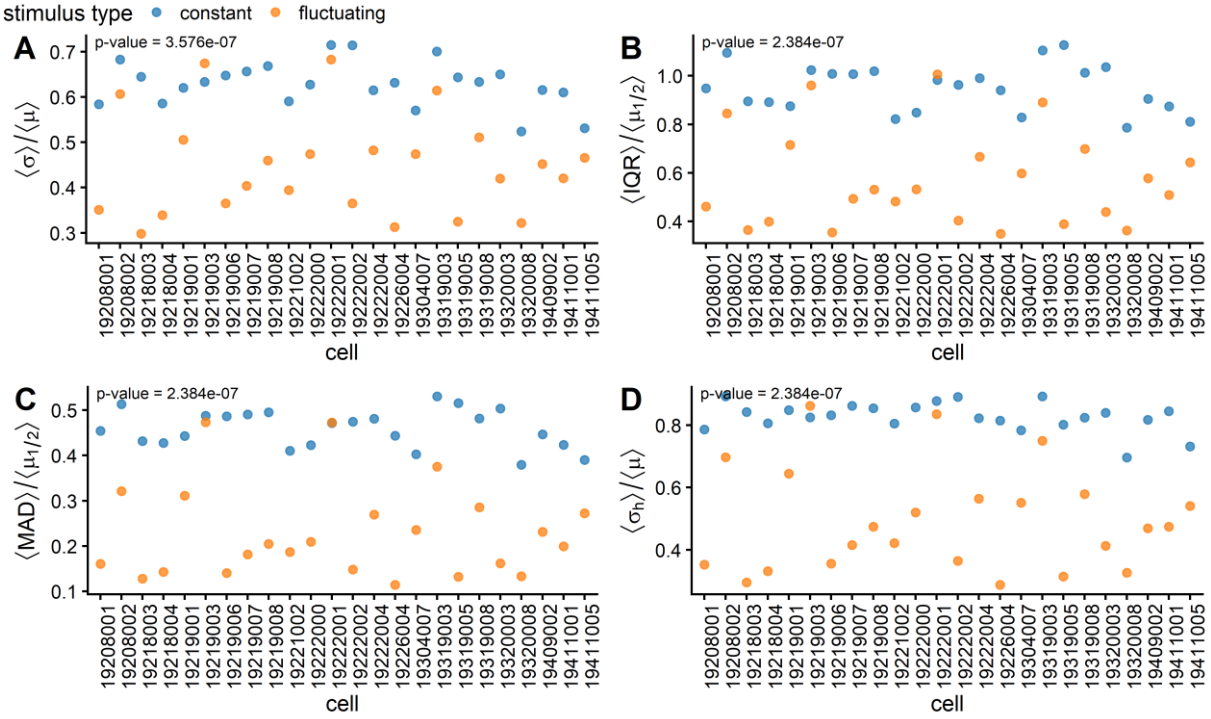

Figure 32: The results for the second type of dispersion measures, i.e., the ratio of the mean dispersion to the mean/median of instantaneous ISIs for individual ORNs.

Finally, we analyze the temporal coding reliability by computing the local variability coefficient L_v (Fig. 11A). That is, for every ORN response trial we obtain one L_v value which describes how variable are the *consequent* ISIs within the spike train. Unlike the *instantaneous* ISI analysis presented above, L_v captures temporal changes in spiking intensity to a much greater extent (Shinomoto, Shima & Tanji, 2003). It is therefore not surprising that the fluctuating stimulus type generates ORN responses with higher L_v. Though the difference is not significant when viewed on the population level (Fig. 33A, p-value ca. 0.4), it is very clear on the level of individual neurons (Fig. 34, p-value ca. 0.001). However, by investigating the standard deviation or even C_v of the local variability L_v, we find out that the intrinsic neuronal noise is actually *smaller* for the fluctuating stimulus type (Figs. 33B and 33C). This trend is then absolutely clear on the scale of individual neurons (Figs. 35 and 36).

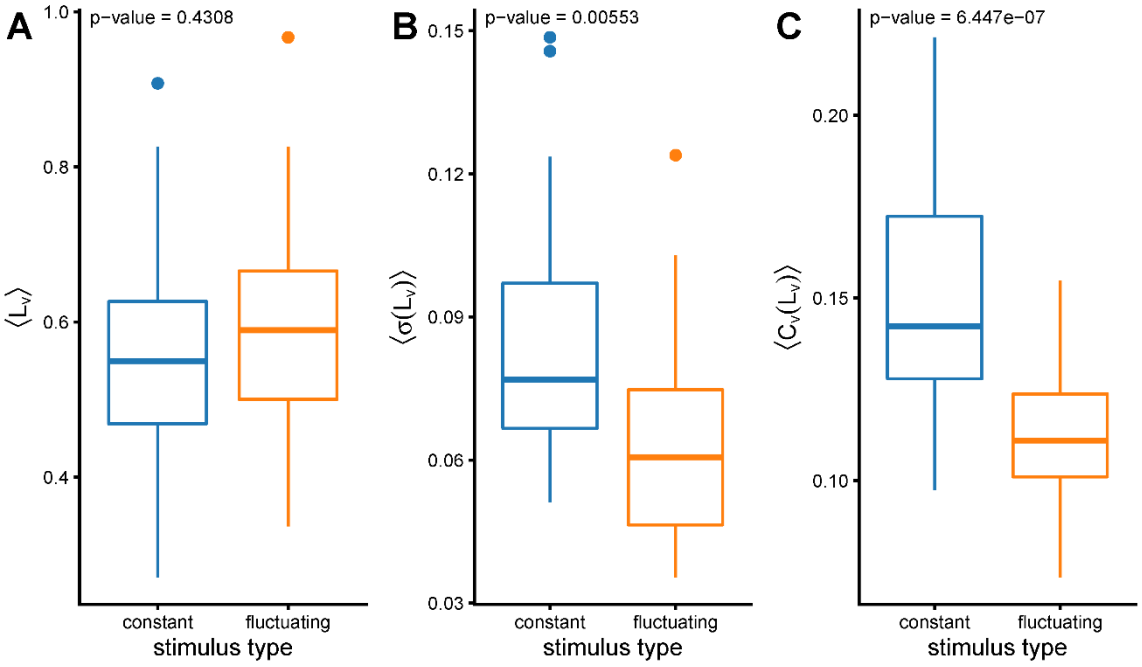

Figure 33: Population results for (A) local variation. Note that there is no significant difference between the two groups, however, Fig. 34 reveals that the LV is actually systematically higher for the fluctuating stimulus type. Both (B) standard deviation of local variation and (C) coefficient of variation of local variation show a significant difference between the groups, which is even more prominent on the level of individual ORNs (Figs. 35 and 36).

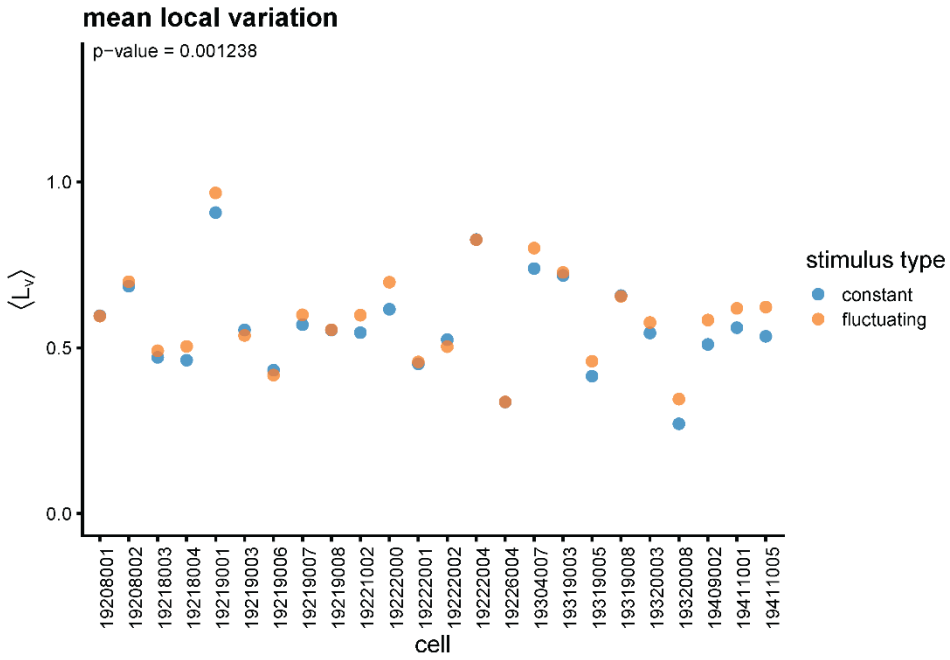

Figure 34: Local variation visualized on the level of individual ORNs. The "fluctuating response" is clearly more variable than the constant one, according to this statistic. It is due to greater temporal changes in spiking intensity within the response to the fluctuating stimulation when compared to the "constant response".

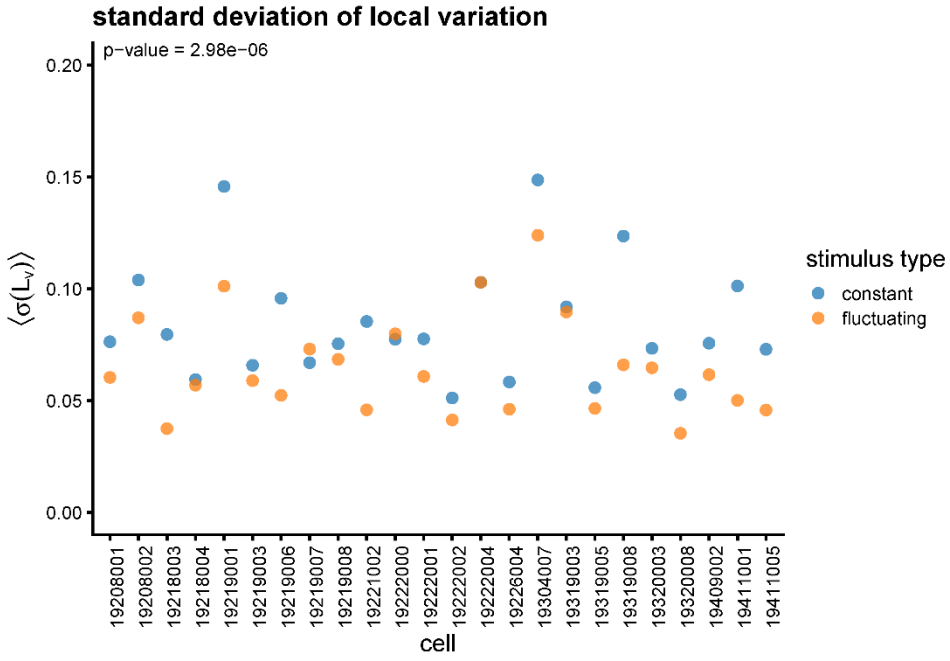

Figure 35: Standard deviation of local variation visualized on the level of individual ORNs. Note that while the average values of LV are higher for the fluctuating stimulus type (see Fig 34), the standard deviation is in fact smaller. In other words, the fluctuating stimulus type leads to a more reproducible response over trials.

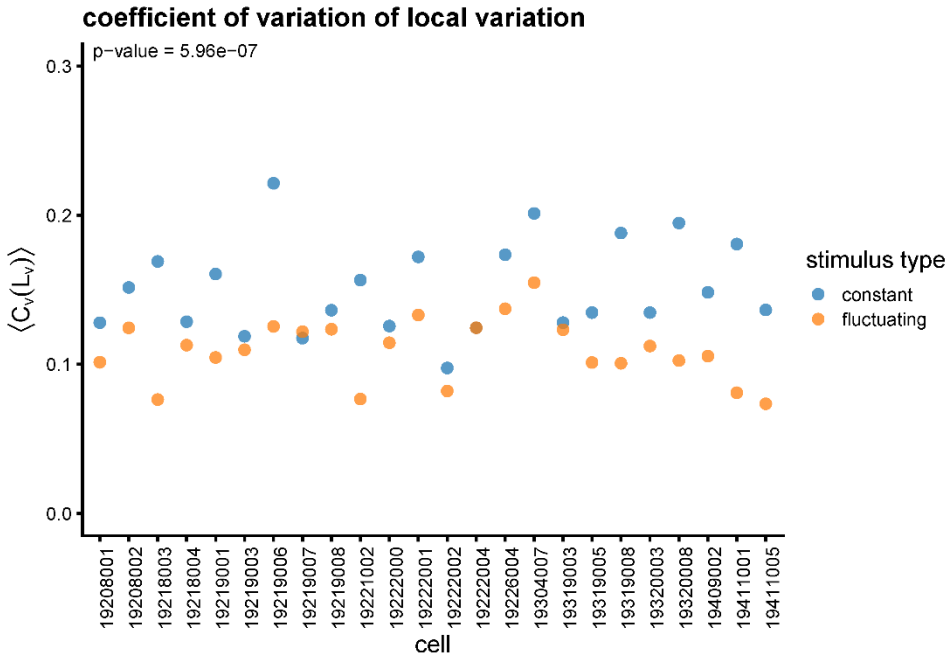

Figure 36: Coefficient of variation of local variation visualized on the level of individual ORNs. This result further confirms and enhances the observations from Fig. 35. Remarkably, although the fluctuating stimulus type leads to a more dynamic response (Fig. 34), the variability of this response is smaller when compared to the less dynamic response to the constant stimulation.

6. Conclusions

A significant portion of this work overviews the subject of computational neuroscience including the problem of neural coding and various approaches to quantifying the reliability of neuronal response. We focus on the efficient coding hypothesis, which represents a powerful organizing principle that has been successfully used in the past, for example, to predict the neuronal receptive fields in the V1 area of the visual cortex (Olshaussen & Field, 1996) or to explain the tuning tune curve properties of the large monopolar cells in the insect compound eye (Laughlin, 1981).

The main subject of this thesis is the first stage of neural coding in the insect olfactory sensory pathway. We are concerned with the special case of the antennal olfactory receptor neurons sensitive to the main pheromone compound of the nocturnal moth *Agrotis ipsilon*. We review the topic of pheromone reception in *Lepidoptera*, including the statistical character of natural stimulation, the architecture of the sensory pathway, and the journey of pheromone molecules from source to receptor. By combining the efficient coding hypothesis with the recent possibility to control precisely the pheromone delivery dynamics in a laboratory setting, we pose the main research task of this thesis, i.e., to investigate and quantify the key aspects of the response reliability to natural-like vs. artificial pheromone stimulation.

In summary, we found that olfactory receptor neurons of moth *Agrotis ipsilon*, respond more reliably to the fluctuating type of stimulation. Because this type of stimulation emulates the stimulation typical for the insect's natural environment, we can conclude that, in the context of our data, the efficient coding hypothesis has been confirmed.

Moreover, our analysis revealed certain unexpected features of the ORN response, some of which can be put into context with recent findings and some of which are novel and require further investigation. We recapitulate these features in the following three points.

First, we report a relatively large spread of all evaluated statistics over the recorded ORN *population*. This observation is consistent with the ORN heterogeneity described in the literature (Rospars et al., 2014). Despite this intrinsic variation, statistics based on entropy show significantly higher response reliability for the fluctuating stimulation.

Second, we found that higher response reliability for the fluctuating stimulation is a universal property of *individual* ORNs. Namely, for both the temporal and the frequency coding schemes and all employed statistical measures of dispersion, almost every ORN responds invariably more reliably to the fluctuating stimulus. This constitutes a novel finding as the population variability may mask the individual ORN coding precision. The cumulative benefits of these separated improvements on the population coding in the antennal lobe warrant further theoretical investigation. We also discuss the properties of different statistical measures and why they provide sufficiently independent perspectives, confirming that our finding is robust.

Third, the possible physiological mechanisms leading to such discrepant reproducibility of the ORN response could not be identified by the employed statistical measures only. However, detailed inspection of individual recordings and their corresponding statistics allows us to state several tentative conclusions. The lower variability of the response during the whiff phase of the fluctuating stimulation can at least partially be attributed to the refractory period when the ORN fires with the maximum possible frequency and ISIs of identical duration. The refractory period itself does not explain the situation for low-frequency neurons. The recently reported post-stimulation inhibition period (Barta et al., 2022) dramatically lowers the variability during the blank phase of fluctuating stimulation, when ORN produces no spikes. We speculate that both these effects jointly contribute to the actual higher response reliability for the natural-like, intermittent pheromone stimulation.

7. Literature

Adrian, E. D., & Zotterman, Y. (1926). The impulses produced by sensory nerve-endings: Part II. The response of a Single End-Organ. *The Journal of Physiology*, 61(2), 151–171.

Ai, H., & Kanzaki, R. (2004). Modular organization of the silkmoth antennal lobe macroglomerular complex revealed by voltage-sensitive dye imaging. *Journal of Experimental Biology*, 207(4), 633–644.

Anton, S., & Homberg, U. (1999). Antennal lobe structure. *Insect olfaction*, 97-124.

Arachchige, C. N., Prendergast, L. A., & Staudte, R. G. (2022). Robust analogs to the coefficient of variation. *Journal of Applied Statistics*, 49(2), 268-290.

Atick, J. J. (1992). Could Information Theory Provide an Ecological Theory of Sensory Processing?. *Network: Computation in Neural Systems* 3(2), 213–251.

Barlow, H. (1961). Possible Principles Underlying the Transformations of Sensory Messages. *Sensory Communication*, 1(01).

Barta, T., C. Monsempes, E. Demondion, A. Chatterjee, L. Kostal, and P. Lucas. (2022). Stimulus Duration Encoding Occurs Early in the Moth Olfactory Pathway. *biorXiv*, (submitted).

Basharin, G. P. (1959) On a statistical estimate for the entropy of a sequence of independent random variables. *Theory of Probability and Its Applications*, 4, 333-336.

Beirlant, J., Dudewicz, E. J., Györfi, L., & Van der Meulen, E. C. (1997). Nonparametric entropy estimation: An overview. *International Journal of Mathematical and Statistical Sciences*, 6(1), 17-39.

Belanger, J. H., & Willis, M. A. (1998, September). Biologically-inspired search algorithms for locating unseen odor sources. *In Proceedings of the 1998 IEEE International Symposium on Intelligent Control (ISIC) held jointly with IEEE*

International Symposium on Computational Intelligence in Robotics and Automation (CIRA) Intell (pp. 265-270). IEEE.

Benton, R., Sachse, S., Michnick, S. W., & Vosshall, L. B. (2006). Atypical membrane topology and heteromeric function of Drosophila odorant receptors in vivo. *PLoS Biology*, 4(2), 240–257.

Benton, R., Vannice, K. S., & Vosshall, L. B. (2007). An essential role for a CD36-related receptor in pheromone detection in Drosophila. *Nature*, 450(7167), 289–293.

Berry, M. J., Warland, D. K., & Meister, M. (1997). The structure and precision of retinal spike trains. *Proceedings of the National Academy of Sciences*, 94(10), 5411-5416.

Bialek, W., and W. G. Owen. (1990). Temporal Filtering in Retinal Bipolar Cells. Elements of an Optimal Computation?. *Biophysical journal* 58(5), 1227–1233.

Boekhoff, I., Strotmann, J., Raming, K., Tareilus, E., & Breer, H. (1990). Odorant-sensitive phospholipase C in insect antennae. *Cellular Signalling*, 2(1), 49–56.

Borst, A., & Theunissen, F. E. (1999). Information theory and neural coding. *Nature Neuroscience*, 2(11), 947–957.

Bryant, H. L., & Segundo, J. P. (1976). Spike initiation by transmembrane current: a white-noise analysis. *The Journal of physiology*, 260(2), 279-314.

Cecchi, G. A., Sigman, M., Alonso, J. M., Martínez, L., Chialvo, D. R., & Magnasco, M. O. (2000). Noise in neurons is message dependent. *Proceedings of the National Academy of Sciences*, 97(10), 5557-5561.

Celani, A., Villermaux, E., & Vergassola, M. (2014). Odor landscapes in turbulent environments. *Physical Review X*, 4(4), 041015.

Dahmen, J. C., Keating, P., Nodal, F. R., Schulz, A. L., & King, A. J. (2010). Adaptation to stimulus statistics in the perception and neural representation of auditory space. *Neuron*, 66(6), 937-948.

Dayan, P., & Abbott, L. F. (2005). Theoretical neuroscience: computational and mathematical modeling of neural systems. MIT press.

Dean, I., Harper, N. S., & McAlpine, D. (2005). Neural population coding of sound level adapts to stimulus statistics. *Nature neuroscience*, 8(12), 1684-1689.

Deneve, S., P. E. Latham, and A. Pouget. 1999. "Reading Population Codes: A Neural Implementation of Ideal Observers." *Nature neuroscience*, 2(8), 740–45.

Deng, Y., Zhang, W., Farhat, K., Oberland, S., Gisselmann, G., & Neuhaus, E. M. (2011). The Stimulatory Gαs Protein Is Involved in Olfactory Signal Transduction in Drosophila. *PLoS One*, 6(4), e18605.

de Ruyter van Steveninck, R. R., Lewen, G. D., Strong, S. P., Koberle, R., & Bialek, W. (1997). Reproducibility and variability in neural spike trains. *Science*, 275(5307), 1805-1808.

Dobritsa, A. A., Van Der Goes Van Naters, W., Warr, C. G., Steinbrecht, R. A., & Carlson, J. R. (2003). Integrating the Molecular and Cellular Basis of Odor Coding in the Drosophila Antenna. *Neuron*, 37(5), 827–841.

Durant, S., Clifford, C. W., Crowder, N. A., Price, N. S., & Ibbotson, M. R. (2007). Characterizing contrast adaptation in a population of cat primary visual cortical neurons using Fisher information. *JOSA A*, 24(6), 1529-1537.

Engsontia, P., Sangket, U., Chotigeat, W., & Satasook, C. (2014). Molecular evolution of the odorant and gustatory receptor genes in lepidopteran insects: implications for their adaptation and speciation. *Journal of Molecular Evolution*, 79(1–2), 21–39.

Esteban, M. D., Castellanos, M. E., Morales, D., & Vajda, I. (2001). Monte Carlo comparison of four normality tests using different entropy estimates. *Communications in Statistics-Simulation and computation*, 30(4), 761-785.

Forstner, M., Breer, H., & Krieger, J. (2009). A receptor and binding protein interplay in the detection of a distinct pheromone component in the silkmoth Antheraea polyphemus. *International Journal of Biological Sciences*, 5(7), 745.

Gallager, R. G. (1968). Information theory and reliable communication (Vol. 588). *New York: Wiley.*

Garcia-Lazaro, J. A., Ho, S. S. M., Nair, A., & Schnupp, J. W. H. (2007). Shifting and scaling adaptation to dynamic stimuli in somatosensory cortex. *European Journal of Neuroscience*, 26(8), 2359-2368.

German, P. F., van der Poel, S., Carraher, C., Kralicek, A. V., & Newcomb, R. D. (2013). Insights into subunit interactions within the insect olfactory receptor complex using FRET. *Insect Biochemistry and Molecular Biology*, 43(2), 138–145.

Gerstner, W., & Kistler, W. M. (2002). Spiking neuron models: Single neurons, populations, plasticity. Cambridge university press.

Gorur-Shandilya, S., Demir, M., Long, J., Clark, D. A., & Emonet, T. (2017). Olfactory receptor neurons use gain control and complementary kinetics to encode intermittent odorant stimuli. *Elife*, 6, e27670.

Große-Wilde, E., Gohl, T., Bouché, E., Breer, H., & Krieger, J. (2007). Candidate pheromone receptors provide the basis for the response of distinct antennal neurons to pheromonal compounds. *European Journal of Neuroscience*, 25(8), 2364–2373.

Guo, H., Huang, L. Q., Pelosi, P., & Wang, C. Z. (2012). Three pheromone-binding proteins help segregation between two Helicoverpa species utilizing the same pheromone components. *Insect Biochemistry and Molecular Biology*, 42(9), 708–716.

Hallem, E. A., Ho, M. G., & Carlson, J. R. (2004). The Molecular Basis of Odor Coding in the Drosophila Antenna. *Cell*, 117(7), 965–979.

Hansson, B. S. (1995). Olfaction in lepidoptera. *Experientia*, *51*(11), 1003-1027.

Hansson, B. S., & Christensen, T. A. (1999). Functional Characteristics of the Antennal Lobe. *Insect Olfaction*, 125–161.

Hillar, C. J., and N. M. Tran. 2018. "Robust Exponential Memory in Hopfield Networks." *The Journal of Mathematical Neuroscience*, 8(1), 1-20.

Hornstein, E. P., O'Carroll, D. C., Anderson, J. C., & Laughlin, S. B. (2000). Sexual dimorphism matches photoreceptor performance to behavioural requirements. *Proceedings of the Royal Society of London. Series B: Biological Sciences*, 267(1457), 2111-2117.

Huber, P. J. 1981. Robust statistics. New York: John Wiley; Sons, Inc.

Ishida, Y., & Leal, W. S. (2005). Rapid inactivation of a moth pheromone. *Proceedings of the National Academy of Sciences*, 102(39), 14075–14079.

Jacob, V., Monsempès, C., Rospars, J. P., Masson, J. B., & Lucas, P. (2017). Olfactory coding in the turbulent realm. *PLoS Computational Biology*, 13(12), e1005870.

Jarriault, D., Gadenne, C., Lucas, P., Rospars, J. P., & Anton, S. (2010). Transformation of the sex pheromone signal in the noctuid moth Agrotis ipsilon: from peripheral input to antennal lobe output. *Chemical senses*, 35(8), 705-715.

Jones, W. D., Nguyen, T. A. T., Kloss, B., Lee, K. J., & Vosshall, L. B. (2005). Functional conservation of an insect odorant receptor gene across 250 million years of evolution. Current Biology, 15(4), R119–R121.

Kaissling, K.-E. (1974). Sensory Transduction in Insect Olfactory Receptors. *Biochemistry of Sensory Functions*, 243–273.

Kaissling, K.-E. (2009). Olfactory perireceptor and receptor events in moths: a kinetic model revised. *Journal of Comparative Physiology A*,195(10), 895–922.

Kaissling, K.-E., Hildebrand, J. G., & Tumlinson, J. H. (1989). Pheromone receptor cells in the male moth Manduca sexta. *Archives of Insect Biochemistry and Physiology*, 10(4), 273–279.

Kaissling, K. E., Kasang, G., Bestmann, H. J., Stransky, W., & Vostrowsky, O. (1978). A new pheromone of the silkworm moth Bombyx mori. *The Science of Nature*, 65(7), 382–384.

Kanaujia, S., & Kaissling, K. E. (1985). Interactions of pheromone with moth antennae: Adsorption, desorption and transport. *Journal of Insect Physiology*, 31(1), 71–81.

Keil, T. (1989). Fine structure of the pheromone-sensitive sensilla on the antenna of the hawkmoth, Manduca sexta. *Tissue & Cell*, 21(1), 139–151.

Keil, T. A. (1999). Morphology and Development of the Peripheral Olfactory Organs. *Insect Olfaction*, 5–47.

Keil, T. A., & Steiner, C. (1991). Morphogenesis of the antenna of the male silkmoth. Antheraea polyphemus, III. Development of olfactory sensilla and the properties of hair-forming cells. *Tissue and Cell*, 23(6), 821–851.

Klein, U. (1987). Sensillum-lymph proteins from antennal olfactory hairs of the moth Antheraea polyphemus (Saturniidae). *Insect Biochemistry*, 17(8), 1193–1204.

Kobayashi, R., Tsubo, Y., & Shinomoto, S. (2009). Made-to-order spiking neuron model equipped with a multi-timescale adaptive threshold. *Frontiers in computational neuroscience*, 3, 9.

Kostal, L., & Kobayashi, R. (2019). Critical size of Neural Population for Reliable Information Transmission. *Physical Review E*, 100(5), 050401.

Kostal, L., & Lansky, P. (2013). Information capacity and its approximations under metabolic cost in a simple homogeneous population of neurons. *Biosystems*, *112*(3), 265-275.

Kostal, L., Lansky, P., & McDonnell, M. D. (2013). Metabolic cost of neuronal information in an empirical stimulus-response model. *Biological cybernetics*, *107*(3), 355-365.

Kostal, L., Lansky, P., & Pokora, O. (2013). Measures of statistical dispersion based on Shannon and Fisher information concepts. *Information Sciences*, 235, 214-223.

Kostal, L., Lansky, P., & Rospars, J. P. (2007). Neuronal coding and spiking randomness. *European Journal of Neuroscience*, 26(10), 2693-2701.

Kostal, L., Lansky, P., & Rospars, J. P. (2008). Efficient olfactory coding in the pheromone receptor neuron of a moth. *PLoS Computational Biology*, 4(4), e1000053.

Kostal, L., Lansky, P., & Stiber, M. (2018). Statistics of inverse interspike intervals: The instantaneous firing rate revisited. *Chaos: An Interdisciplinary Journal of Nonlinear Science*, 28(10), 106305.

Kostal, L., & Pokora, O. (2012). Nonparametric estimation of information-based measures of statistical dispersion. *Entropy*, 14(7), 1221-1233.

Krieger, J., Große-Wilde, E., Gohl, T., & Breer, H. (2005). Candidate pheromone receptors of the silkmoth Bombyx mori. *European Journal of Neuroscience*, 21(8), 2167–2176.

Krieger, J., Grosse-Wilde, E., Gohl, T., Dewer, Y. M. E., Raming, K., & Breer, H. (2004). Genes encoding candidate pheromone receptors in a moth (Heliothis virescens). *Proceedings of the National Academy of Sciences*, 101(32), 11845–11850.

Krieger, J., Klink, O., Mohl, C., Raming, K., & Breer, H. (2003). A candidate olfactory receptor subtype highly conserved across different insect orders. *Journal of Comparative Physiology A*, 189(7), 519–526.

Kupper, R., Gewaltig, M. O., Körner, U., & Körner, E. (2005). Spike-latency codes and the effect of saccades. *Neurocomputing*, 65, 189–194.

Larsson, M. C., Domingos, A. I., Jones, W. D., Chiappe, M. E., Amrein, H., & Vosshall, L. B. (2004). Or83b Encodes a Broadly Expressed Odorant Receptor Essential for Drosophila Olfaction. *Neuron*, 43(5), 703–714.

Laughlin, S. (1981). A simple coding procedure enhances a neuron's information capacity. *Zeitschrift fur Naturforschung c*, 36(9-10), 910-912.

Laughlin, S. B. (1996). Matched filtering by a photoreceptor membrane. *Vision research*, 36(11), 1529-1541.

Leal, W. S., Chen, A. M., Ishida, Y., Chiang, V. P., Erickson, M. L., Morgan, T. I., & Tsuruda, J. M. (2005). Kinetics and molecular properties of pheromone binding and release. *Proceedings of the National Academy of Sciences*, *102*(15), 5386-5391.

Lee, J. K., & Strausfeld, N. J. (1990). Structure, distribution and number of surface sensilla and their receptor cells on the olfactory appendage of the male moth Manduca sexta. *Journal of Neurocytology*, 19(4), 519-538.

Levakova, M., Kostal, L., Monsempès, C., Jacob, V., & Lucas, P. (2018). Moth olfactory receptor neurons adjust their encoding efficiency to temporal statistics of pheromone fluctuations. *PLoS computational biology*, *14*(11), e1006586.

Lewicki, M. S. (2002). Efficient coding of natural sounds. *Nature neuroscience*, 5(4), 356-363.

Lundin, C., Käll, L., Kreher, S. A., Kapp, K., Sonnhammer, E. L., Carlson, J. R., Heijne, G. von, & Nilsson, I. M. (2007). Membrane topology of the Drosophila OR83b odorant receptor. *FEBS Letters*, 581(29), 5601–5604.

Maass, W. (1997). Networks of Spiking Neurons: The Third Generation of Neural Network Models. *Neural Networks*, 10(9): 1659–1671.

Machens, C. K., Gollisch, T., Kolesnikova, O., & Herz, A. V. (2005). Testing the efficiency of sensory coding with optimal stimulus ensembles. *Neuron*, 47(3), 447-456.

MacKay, D. M., & McCulloch, W. S. (1952). The limiting information capacity of a neuronal link. *The bulletin of mathematical biophysics*, 14(2), 127-135.

Maida, R., Ziegelberger, G., & Kaissling, K.-E. (2003). Ligand binding to six recombinant pheromone-binding proteins of Antheraea polyphemus and Antheraea pernyi. *Journal of Comparative Physiology B*, 7(173), 565–573.

Maier, J. K., Hehrmann, P., Harper, N. S., Klump, G. M., Pressnitzer, D., & McAlpine, D. (2012). Adaptive coding is constrained to midline locations in a spatial listening task. *Journal of Neurophysiology*, 108(7), 1856-1868.

Mainen, Z. F., & Sejnowski, T. J. (1995). Reliability of spike timing in neocortical neurons. *Science*, 268(5216), 1503-1506.

McCulloch, W. S., & Pitts, W. (1943). A logical calculus of the ideas immanent in nervous activity. *The bulletin of mathematical biophysics*, 5(4), 115-133.

Michel, E., Damberger, F. F., Ishida, Y., Fiorito, F., Lee, D., Leal, W. S., & Wüthrich, K. (2011). Dynamic Conformational Equilibria in the Physiological Function of the Bombyx mori Pheromone-Binding Protein. *Journal of Molecular Biology*, 408(5), 922–931.

Miller, E. G., & Fisher, J. W. (2003). ICA using spacings estimates of entropy. *The Journal of Machine Learning Research*, *4*, 1271-1295.

Murlis, J. (1996). Odor Plumes and the Signal They Provide. *Insect Pheromone Research: New Directions*, edited by R. T. Carde and A. Minks, 221–31. New York: Chapman; Hall.

Murlis, J., Willis, M. A., & Cardé, R. T. (2000). Spatial and temporal structures of pheromone plumes in fields and forests. *Physiological entomology*, 25(3), 211-222.

Nakagawa, T., & Vosshall, L. B. (2009). Controversy and consensus: noncanonical signaling mechanisms in the insect olfactory system. *Current Opinion in Neurobiology*, 19(3), 284–292.

Nawrot, M., Aertsen, A., & Rotter, S. (1999). Single-trial estimation of neuronal firing rates: from single-neuron spike trains to population activity. *Journal of neuroscience methods*, 94(1), 81-92.

Nichols, A. S., Chen, S., & Luetje, C. W. (2011). Subunit Contributions to Insect Olfactory Receptor Function: Channel Block and Odorant Recognition. *Chemical Senses*, 36(9), 781–790.

Nolte, A., Funk, N. W., Mukunda, L., Gawalek, P., Werckenthin, A., Hansson, B. S., Wicher, D., & Stengl, M. (2013). In situ Tip-Recordings Found No Evidence for an Orco-Based Ionotropic Mechanism of Pheromone-Transduction in Manduca sexta. *PLoS One*, 8(5), e62648.

Nolte, A., Gawalek, P., Koerte, S., Wei, H., Schumann, R., Werckenthin, A., Krieger, J., & Stengl, M. (2016). No Evidence for Ionotropic Pheromone Transduction in the Hawkmoth Manduca sexta. *PLoS One*, 11(11), e0166060.

O'Keefe, J. (1993). Hippocampus, theta, and spatial memory. Current Opinion in *Neurobiology*, 3(6), 917–924.

Olshausen, B. A., & Field, D. J. (1996). Emergence of simple-cell receptive field properties by learning a sparse code for natural images. *Nature*, *381*(6583), 607-609.

Perkel, D. H., & Bullock, T. H. (1968). Neural coding. *Neurosciences Research Program Bulletin*, 6(3), 221–348.

Perkel, D. H., Gerstein, G. L., & Moore, G. P. (1967a). Neuronal spike trains and stochastic point processes: I. The single spike train. *Biophysical journal*, 7(4), 391-418.

Perkel, D. H., Gerstein, G. L., & Moore, G. P. (1967b). Neuronal spike trains and stochastic point processes: II. Simultaneous spike trains. Biophysical journal, 7(4), 419-440.

Rospars, J. P., Grémiaux, A., Jarriault, D., Chaffiol, A., Monsempes, C., Deisig, N., ... & Martinez, D. (2014). Heterogeneity and convergence of olfactory first-order neurons account for the high speed and sensitivity of second-order neurons. *PLoS computational biology*, *10*(12), e1003975.

Sakurai, T., Mitsuno, H., Mikami, A., Uchino, K., Tabuchi, M., Zhang, F., Sezutsu, H., & Kanzaki, R. (2015). Targeted disruption of a single sex pheromone receptor gene

completely abolishes in vivo pheromone response in the silkmoth. *Scientific Reports*, 5(1), 1–11.

Sakurai, T., Nakagawa, T., Mitsuno, H., Mori, H., Endo, Y., Tanoue, S., Yasukochi, Y., Touhara, K., & Nishioka, T. (2004). Identification and functional characterization of a sex pheromone receptor in the silkmoth Bombyx mori. *Proceedings of the National Academy of Sciences*, 101(47), 16653–16658.

Sato, K., Pellegrino, M., Nakagawa, T., Nakagawa, T., Vosshall, L. B., & Touhara, K. (2008). Insect olfactory receptors are heteromeric ligand-gated ion channels. *Nature*, 452(7190), 1002–1006.

Sejnowski, T. J., Koch, C., & Churchland, P. S. (1988). Computational Neuroscience. *Science*, 241(4871), 1299–1306.

Shinomoto, S., Miura, K., & Koyama, S. (2005). A measure of local variation of inter-spike intervals. *BioSystems*, 79(1-3), 67–72.

Shinomoto, S., Shima, K., & Tanji, J. (2003). Differences in Spiking Patterns among Cortical Neurons. *Neural Computation*, 15(12), 2823–2842.

Simoncelli, E. P., & Olshausen, B. (2001). Natural image statistics and neural representation. *Annual review of neuroscience*, 24(1), 1193-1216.

Smart, R., Kiely, A., Beale, M., Vargas, E., Carraher, C., Kralicek, A. V., Christie, D. L., Chen, C., Newcomb, R. D., & Warr, C. G. (2008). Drosophila odorant receptors are novel seven transmembrane domain proteins that can signal independently of heterotrimeric G proteins. *Insect Biochemistry and Molecular Biology*, 38(8), 770–780.

Smith, E. C., & Lewicki, M. S. (2006). Efficient auditory coding. *Nature*, 439(7079), 978-982.

Stein, R. B., Gossen, E. R., & Jones, K. E. (2005). Neuronal variability: Noise or part of the signal?. *Nature Reviews Neuroscience*, 6(5), 389-397.

Steinbrecht, R. A. (1997). Pore structures in insect olfactory sensilla: A review of data and concepts. *International Journal of Insect Morphology and Embryology*, 26(3-4), 229-245.

Stengl, M. (1993). Intracellular-messenger-mediated cation channels in cultured olfactory receptor neurons. *Journal of Experimental Biology*, 178(1), 125–147.

Stengl, M. (1994). Inositol-trisphosphate-dependent calcium currents precede cation currents in insect olfactory receptor neurons in vitro. *Journal of Comparative Physiology A*, 174(2), 187–194.

Stengl, M. (2010). Pheromone transduction in moths. Frontiers in Cellular *Neuroscience*, 4(DEC), 133.

Stengl, M., & Funk, N. W. (2013). The role of the coreceptor Orco in insect olfactory transduction. *Journal of Comparative Physiology A*, 199(11), 897–909.

Stengl, M., Zufall, F., Hatt, H., & Hildebrand, J. G. (1992). Olfactory receptor neurons from antennae of developing male Manduca sexta respond to components of the species-specific sex pheromone in vitro. *Journal of Neuroscience*, 12(7), 2523–2531.

Stöckl, C., and W. Maass (2021). Optimized Spiking Neurons Can Classify Images with High Accuracy Through Temporal Coding with Two Spikes. *Nature Machine Intelligence*, 3(3): 230–238.

Theunissen, F., & Miller, J. P. (1995). Temporal encoding in nervous systems: a rigorous definition. *Journal of computational neuroscience*, 2(2), 149-162.

Thorpe, S., Fize, D., & Marlot, C. (1996). Speed of processing in the human visual system. *Nature*, 381(6582), 520–522.

van Hateren, J. H. (1992). Theoretical predictions of spatiotemporal receptive fields of fly LMCs, and experimental validation. *Journal of Comparative Physiology A*, 171(2), 157-170.

Vasicek, O. (1976). A test for normality based on sample entropy. *Journal of the Royal Statistical Society: Series B (Methodological)*, 38(1), 54-59.

Vogt, R. G., & Riddiford, L. M. (1981). Pheromone binding and inactivation by moth antennae. *Nature*, 293(5828), 161–163.

Vogt, R. G., Riddiford, L. M., & Prestwich, G. D. (1985). Kinetic properties of a sex pheromone-degrading enzyme: the sensillar esterase of Antheraea polyphemus. *Proceedings of the National Academy of Sciences*, 82(24), 8827–8831.

Vosshall, L. B., Amrein, H., Morozov, P. S., Rzhetsky, A., & Axel, R. (1999). A Spatial Map of Olfactory Receptor Expression in the Drosophila Antenna. *Cell*, 96(5), 725–736.

Vosshall, L. B., & Hansson, B. S. (2011). A Unified Nomenclature System for the Insect Olfactory Coreceptor. *Chemical Senses*, 36(6), 497–498.

Wark, B., Lundstrom, B. N., & Fairhall, A. (2007). Sensory adaptation. *Current opinion in neurobiology*, 17(4), 423-429.

Warzecha, A. K., & Egelhaaf, M. (1999). Variability in spike trains during constant and dynamic stimulation. *Science*, 283(5409), 1927-1930.

Watkins, P. V., & Barbour, D. L. (2008). Specialized neuronal adaptation for preserving input sensitivity. *Nature neuroscience*, 11(11), 1259-1261.

Watkins, P. V., & Barbour, D. L. (2011). Level-tuned neurons in primary auditory cortex adapt differently to loud versus soft sounds. *Cerebral Cortex*, 21(1), 178-190.

Wen, B., Wang, G. I., Dean, I., & Delgutte, B. (2009). Dynamic range adaptation to sound level statistics in the auditory nerve. *Journal of Neuroscience*, 29(44), 13797-13808.

Wicher, D., Schäfer, R., Bauernfeind, R., Stensmyr, M. C., Heller, R., Heinemann, S. H., & Hansson, B. S. (2008). Drosophila odorant receptors are both ligand-gated and cyclic-nucleotide- activated cation channels. *Nature*, 452(7190), 1007–1011.

Xu, W., & Leal, W. S. (2008). Molecular switches for pheromone release from a moth pheromone-binding protein. *Biochemical and Biophysical Research Communications*, 372(4), 559–564.

Zenke, F., S. M. Bohté, C. Clopath, I. M. Comşa, J. Göltz, W. Maass, T. Masquelier, et al. (2021). Visualizing a Joint Future of Neuroscience and Neuromorphic Engineering. *Neuron*, 109(4), 571–75.